LBL-14074
Preprint c.2

# Lawrence Berkeley Laboratory
UNIVERSITY OF CALIFORNIA

RECEIVED
LAWRENCE
BERKELEY LABORATORY

JUL 15 1982

LIBRARY AND
DOCUMENTS SECTION

Submitted to Nuclear Physics

DYNAMICAL ASPECTS OF NUCLEUS-NUCLEUS COLLISIONS

S. Bjørnholm and W.J. Swiatecki

May 1982

TWO-WEEK LOAN COPY

*This is a Library Circulating Copy which may be borrowed for two weeks. For a personal retention copy, call Tech. Info. Division, Ext. 6782.*

NUCLEAR SCIENCE DIVISION

LBL-14074 c.2

Prepared for the U.S. Department of Energy under Contract DE-AC03-76SF00098

## DISCLAIMER

This document was prepared as an account of work sponsored by the United States Government. While this document is believed to contain correct information, neither the United States Government nor any agency thereof, nor the Regents of the University of California, nor any of their employees, makes any warranty, express or implied, or assumes any legal responsibility for the accuracy, completeness, or usefulness of any information, apparatus, product, or process disclosed, or represents that its use would not infringe privately owned rights. Reference herein to any specific commercial product, process, or service by its trade name, trademark, manufacturer, or otherwise, does not necessarily constitute or imply its endorsement, recommendation, or favoring by the United States Government or any agency thereof, or the Regents of the University of California. The views and opinions of authors expressed herein do not necessarily state or reflect those of the United States Government or any agency thereof or the Regents of the University of California.

LBL-14074

# Dynamical Aspects of Nucleus-Nucleus Collisions

S. Bjørnholm

Niels Bohr Institute, Blegdamsvej 17
DK-2100 Copenhagen Ø, Denmark

and

W.J. Swiatecki

Nuclear Science Division, Lawrence Berkeley Laboratory
University of California, Berkeley, CA 94720

This work was supported by the Director, Office of Energy Research, Division of Nuclear Physics of the Office of High Energy and Nuclear Physics of the U.S. Department of Energy under Contract DE-AC03-76SF00098 and by the Danish Natural Sciences Council.

LBL-14074

# Dynamical Aspects of Nucleus-Nucleus Collisions

S. Bjørnholm

Niels Bohr Institute, Blegdamsvej 17
DK-2100 Copenhagen Ø, Denmark

and

W.J. Swiatecki

Nuclear Science Division, Lawrence Berkeley Laboratory
University of California, Berkeley, CA 94720

## Abstract

This is an extension of the macroscopic theory of nucleus-nucleus reactions described in Ref. 17. The fusion or reseparation of two colliding nuclei is treated according to a schematic model based on the "Chaotic Regime Dynamics" (liquid-drop potential energy plus one-body dissipation). Attention is focused on three hurdles or "milestone configurations" that a colliding system may be faced with: the touching configuration, the conditional saddle-point configuration at frozen mass asymmetry, and the unconditional saddle-point configuration. Semi-empirical formulae are derived for the "Extra Push" (the extra energy needed in some situations to carry the system from the first to the second hurdle) and for the "Extra-extra Push" (the energy needed to carry the system from the first to the third hurdle). The theoretical formulae are confronted with measurements of fusion and evaporation-residue cross sections. A discussion of the implications for superheavy-element reactions is given, using the production of element 107 in the bombardment of $^{209}$Bi with $^{54}$Cr as a calibrating reaction.

## 1. Introduction

It is becoming more and more apparent that the nature of nuclear macroscopic shape dynamics is profoundly affected by the symmetries of the configurations in question (Refs. 1,2,4). On the one hand, if the nuclear configuration is free of symmetries (the "Chaotic Regime") the static potential energy, considered as a function of shape, is now known to be described quite accurately by a leptodermous (liquid-drop) type of expression (Refs. 2-9) and, although this is by no means established, the dynamics of shape changes is expected to follow a simple equation of motion, based on the one-body dissipation concept (Refs. 1,2,10,11). The resulting shape dynamics is predicted to be severely overdamped: the nucleus should behave like a viscous fluid, with a novel type of viscosity, described by the Wall or Wall-and-Window Formula (Refs. 10,11,12). On the other hand, when the nuclear system is dominated by symmetries, the single-particle level structure of the nucleons acquires special features (bunching and crossing or near-crossing of levels) and the nucleus becomes more like a visco-elastic solid, in some cases actually dominated by elasticity.* This symmetry-dominated regime of nuclear dynamics has been vividly illustrated by the prediction, discovery, and further elucidation of the giant quadrupole resonances (Ref. 14). Adding to this the striking pair correlation effects associated with time-reversal symmetry (responsible for superconductivity and superfluidity in macroscopic

---

* Many of these ideas are present in the seminal paper of Hill and Wheeler, dating back to 1953 (Ref. 13). Thus, the notion of a shape-dependent viscosity, related to symmetries, is mentioned on p. 1115, and the two different kinds of shape stiffness, one like that of a fluid and the other like that of a solid, may be deduced from a corrected version of Fig. 12. (See Ref. 4, Fig. 7.) An attempt to derive a "Wall Formula" for energy dissipation is also present on pp. 1123, 1138.

bodies) it is clear that nuclear dynamics is a fascinatingly rich and complex field for study of which, at the moment, we only possess an approximate understanding of a few especially simple limiting cases.

The theoretical exploration of the limiting case corresponding to the dissipation-dominated Chaotic Regime, initiated half a dozen years ago, has been confronted in the past with experimental data on nuclear fission and deep-inelastic reactions (Refs. 2,10,15,16). Very recently, striking contacts between a schematic model incorporating the Chaotic Regime dynamics and fusion experiments have been made (Refs. 17-22,27). These confrontations of theory and experiment center around the existence of an "extra push" necessary to make two sufficiently heavy nuclei fuse and an "extra-extra push" to make a compound nucleus. In the present paper we analyze further the consequences of the schematic model introduced in Ref. 12 and we discuss the expected excitation functions for nucleus-nucleus reactions classified into four types: elastic (and quasi-elastic) reactions, dinucleus (deep-inelastic) reactions, mononucleus (fast-fission) reactions, and compound nucleus reactions.

We should stress at the outset that, in view of the anticipated richness of the true nuclear dynamics, the present study is carried out in the spirit of taking a simple model based on a limiting idealization and confronting it with experiment, fully expecting that significant deviations ought to appear. But since it is by no means easy to predict the extent of the deviations from the Chaotic Regime Dynamics that symmetries (including pairing) will produce, we believe that a comparison of even this very idealized dynamics with experimental data should be informative.

## 2. The Extra Push and the Extra-Extra Push

The schematic model of Ref. 12 illustrated the expectation that there should often be three configurations of special importance--three milestones--in the dynamical evolution of a nucleus-nucleus collision. These three milestone configurations, which define three associated threshold energies, are as follows:

I. The Contact Configuration, where the two nuclei come into contact and the growth of a neck between them becomes energetically favourable. This type I configuration is usually close to the top of the interaction barrier in a one-dimensional plot of the potential energy of two approaching nuclei, whose densities are assumed to be frozen. (It would coincide exactly with the top of the barrier if the nuclear surfaces were sharp and the range of nuclear forces were neglected.) However, for systems with sufficient electric charge and/or angular momentum, the maximum in the (effective) interaction may disappear, but the contact configuration is expected to retain its milestone significance, associated with the rather sudden unfreezing of the neck degree of freedom around contact.

II. The Configuration of Conditional Equilibrium (a saddle-point pass) in a multidimensional plot of the potential energy at frozen mass asymmetry. (The equilibrium is conditional because its energy is stationary only on condition that the asymmetry be held fixed.) The physical significance of this Type II milestone is proportional to the degree of inhibition of the mass-asymmetry degree of freedom, which in turn is related to the severity of the constriction (the smallness of the neck) in the conditional equilibrium shape. When the constriction is not severe, in particular when the shape is convex everywhere, the Type II configuration loses its physical significance as a milestone configuration.

III. The Configuration of Unconditional Equilibrium (the fission saddle-point shape). The associated fission barrier ensures the existence of a compound nucleus and guards it against disintegration. For a system with sufficient electric charge and/or angular momentum, the fission barrier disappears and a compound nucleus ceases to exist.

The Type II and Type III configurations are identical for mass-symmetric systems. They become substantially different only for sufficiently asymmetric systems.

In cases when all three milestone configurations exist, are distinct and physically significant, the three associated threshold energies suggest a division of nucleus-nucleus reactions into four more or less distinct categories (see Fig. 1):

1. Reactions whose dynamical trajectories in configuration space do not overcome the type I threshold (i.e. trajectories that do not bring the nuclei into contact) lead to binary reactions (elastic and quasi-elastic scattering).

2. Trajectories that overcome threshold I but not thresholds II and III, correspond to dinuclear (deep-inelastic) reactions.

3. Trajectories that overcome thresholds I and II but not III correspond to mononucleus (fast-fission) reactions.

4. Trajectories that overcome thresholds I, II, and III (and are trapped inside barrier III) correspond to compound-nucleus reactions.

We may note that in the idealization where the nuclear surfaces are assumed to be sharp and the range of nuclear forces is disregarded, there would be a clear-cut distinction between deep-inelastic and elastic reactions (looking apart, that is, from inelasticities induced by electromagnetic interactions). This is illustrated in the model of Ref. 12 where, in Fig. 6, trajectories that have resulted in contact are discontinuously different from

those that have not. (The latter correspond to motion back and forth along the $\rho$-axis in Fig. 6 of Ref. 12.) This leaves a blank space between the last elastic trajectory and the first deep-inelastic trajectory. With the diffuseness of the nuclear surfaces taken into account, this blank space would be filled out with trajectories that vary from binary (elastic) to dinucleus (deep-inelastic) reactions in a way that washes out the original discontinuity. The degree of washing out is, however, proportional to the diffuseness of the surfaces, and it should be possible to maintain an approximate but useful distinction between elastic and deep-inelastic reactions to the extent that the leptodermous (thin-skin) approach to nuclear processes is approximtely valid.

The qualitative consequences of the existence of the three milestone configurations were illustrated in the model of Ref. 12. The physical ingredients of that model were

1. Conservative driving forces derived from a leptodermous (liquid-drop) potential energy,

2. Dissipative forces derived from the chaotic-regime, one-body dissipation function in the form of the wall or wall-and-window formula,

3. A schematic (reduced-mass) inertial force in the approach degree of freedom.

The model was further simplified by assuming the nuclear shapes to be parametrized as two spheres connected by a portion of a cone and by relying heavily on the small-neck approximation.

One consequence of the above model, which is obvious from qualitative considerations and had already been studied for symmetric systems in Ref. 23, is that for relatively light reacting nuclei the overcoming of the threshold I is sufficient to overcome barrier II, but that for heavier systems, or for

systems with sufficient angular momentum, an "extra push" (an extra radial injection velocity over the threshold condition I) is necessary. Figure 2a (identical with Fig. 5 in Ref. 17) illustrates the dependence of the extra push (in MeV and for head-on collisions) on the atomic numbers $Z_1$, $Z_2$ of the reacting nuclei. In the schematic model used to construct the figure there emerges an approximate small-neck scaling parameter, the "effective fissility parameter" $x_{eff}$, proportional to the effective fissility $(Z^2/A)_{eff}$, and given by

$$x_{eff} = (Z^2/A)_{eff} \Big/ (Z^2/A)_{crit} \quad , \tag{1}$$

where

$$(Z^2/A)_{eff} \equiv \frac{4Z_1Z_2}{A_1^{1/3}A_2^{1/3}(A_1^{1/3}+A_2^{1/3})} \quad , \tag{2}$$

$$(Z^2/A)_{crit} \equiv \frac{40\pi\gamma r_o^3}{3e^2} \quad , \tag{3}$$

$$\gamma = \gamma_o(1 - \kappa_s I^2) \quad . \tag{4}$$

In the above, $\gamma_o$ is the surface-energy coefficient of standard nuclear matter, $I = (N-Z)/A$ is the relative neutron excess, e is the unit of charge, and $\kappa_s$ is the surface-symmetry energy coefficient. Using Ref. 9 we have

$$4\pi r_o^2\gamma_o = 17.9439 \text{ MeV}$$

$$\frac{3}{5}\frac{e^2}{r_o} = 0.7053 \text{ MeV}$$

$$\kappa_s = 1.7826 \quad ,$$

where $r_o$ is the nuclear radius parameter. It follows that an approximate expression for $(Z^2/A)_{crit}$ is

$$(Z^2/A)_{crit} = 50.883(1 - 1.7826\ I^2) \quad . \tag{5}$$

The parameter $x_{eff}$, proportional to Bass' parameter x (Ref. 24), is a measure of the relative importance of electric and nuclear forces for necked-in configurations near contact. Its usefulness is illustrated by the fact that loci of equal extra push in Fig. 2a are approximately loci of equal $x_{eff}$ (approximately also loci of equal $(Z^2/A)_{eff}$).

The schematic model of Ref. 12 was also used to map out the "extra-extra push" over the interaction barrier, needed to overcome the unconditional barrier III (and form a compound nucleus). The result was presented in Fig. 6 of Ref. 17 and is reproduced here as Fig. 2b. For symmetric systems (along the diagonal $Z_1 = Z_2$) and in the region marked "beach" in Fig. 2b, the extra-extra push is identical with the extra push, but for asymmetric systems, above the "cliff", the extra-extra push exceeds the extra push. One verifies readily that the loci of equal extra-extra push are no longer, even approximately, loci of equal $x_{eff}$ or $(Z^2/A)_{eff}$. The reason is that, in the assault on the unconditional barrier III, the fusing system traverses regions of configuration space where its shape has no well-defined neck or asymmetry and the small-neck scaling parameter $x_{eff}$ is no longer relevant. In those regions the standard (total) fissility parameter x (or $(Z^2/A)$), where

$$x = (Z^2/A)/(Z^2/A)_{crit} \quad , \tag{6}$$

is the appropriate scaling parameter. Since, however, the trajectories in question traverse both the dinuclear and mononuclear regimes, neither x nor $x_{eff}$ can be expected to be good scaling parameters. (In Fig. 2b loci of constant x or $(Z^2/A)$ would be approximately parallel straight lines corresponding to $Z_1 + Z_2$ = constant.)

The above circumstance appeared to put a serious limitation on a simple scaling-type exploitation of the results presented in Fig. 2b, until we realized that the use of a mean scaling parameter $x_m$, defined as a suitable mean between x and $x_{eff}$, reproduced approximately the loci of the calculated extra-extra push. A fair representation is obtained by taking $x_m$ to be simply the geometric mean, $x_g$, between x and $x_{eff}$ (written $x_e$ from now on), viz.:

$$x_m \approx x_g = \sqrt{xx_e} \propto \sqrt{(Z^2/A)(Z^2/A)_e} \quad . \tag{7}$$

A more flexible parametrization of the model calculations is obtained by making $x_m$ deviate more rapidly from x with increasing asymmetry. Since the deviation of $x_g$ from x is, in fact, itself a measure of asymmetry*, we have tried the following definition of $x_m$:

$$x_m = x\left[1 - \left(\frac{x-x_g}{x}\right) - k\left(\frac{x-x_g}{x}\right)^2\right] \tag{8}$$

$$= x_g - kx\left(\frac{x-x_g}{x}\right)^2 \quad , \tag{9}$$

i.e.

$$\frac{x_m - x_g}{x} = -k\left(\frac{x-x_g}{x}\right)^2 \quad ,$$

---

*It may be verified from eq. (10) in Ref. 12 that $(x-x_g)/x$ is equal to $1 - (1 - D)(1 + 3D)^{-1/2} \approx (5/2)D$, where D is a measure of asymmetry, given by the square of the difference between the fragment radii divided by their sum, i.e. $D = [(R_1-R_2)/(R_1+R_2)]^2$.

where k will be regarded as an adjustable parameter, controlling the deviation of $x_m$ from $x_g$. Using an appropriate value of k we then constructed Fig. 2c according to the procedure explained in what follows.

We start with the formula for the extra push (denoted by $E_x$), which is obtained, according to eq. (29) in Ref. 12, by writing the extra relative injection velocity -dr/dt, expressed in the natural velocity unit of the one-body dissipation dynamics, as a function, $\phi$, of the excess of the effective fissility parameter $x_e$ over a threshold value $x_{th}$:

$$\frac{-dr/dt}{(2\gamma/\rho\bar{v}\bar{R})} = \phi(x_e - x_{th}) \tag{10}$$

$$\approx a(x_e - x_{th}) + \text{higher powers of } (x_e - x_{th}) \quad , \tag{11}$$

where

$$a = \left.\frac{d\phi}{dx_e}\right|_{x_e=x_{th}} \quad . \tag{12}$$

Here $\rho$ is the nuclear matter density, $\bar{v}$ the mean nucleonic speed, $\bar{R}$ the reduced radius of the system $[\bar{R} = R_1R_2/(R_1+R_2)]$ and $\underline{a}$ is a constant (the derivative of $\phi$ evaluated at $x_e = x_{th}$). The threshold fissility parameter $x_{th}$ is a universal constant. The corresponding threshold value of $(Z^2/A)_{th}$ is given by

$$(Z^2/A)_{th} = x_{th}(Z^2/A)_{crit} \quad . \tag{13}$$

Note that a fixed value of $x_{th}$ would imply a fixed value of $(Z^2/A)_{th}$ only if the surface energy coefficient in eq. (3) were a constant. Since, in fact, $\gamma$ depends somewhat on the neutron excess, the threshold value of $(Z^2/A)_{th}$ is, in general, <u>not quite the same for different nuclear systems</u>.

Denoting the reduced mass of the colliding system by $M_r$, we find for $E_x$ the expression

$$E_x = \frac{1}{2} M_r \left(\frac{dr}{dt}\right)^2 = E_{ch}\, \phi^2 \quad , \tag{14}$$

where $E_{ch}$ is a characteristic energy unit of the system, given by

$$E_{ch} = \frac{2048}{81}\left(\frac{\pi}{3}\right)^{4/3} \frac{m\gamma^2 r_o^6}{\hbar^2} \frac{A_1^{1/3}A_2^{1/3}(A_1^{1/3}+A_2^{1/3})^2}{A}$$

$$= \frac{32}{2025}\left(\frac{3}{\pi}\right)^{2/3} \frac{me^4}{\hbar^2} \frac{A_1^{1/3}A_2^{1/3}(A_1^{1/3}+A_2^{1/3})^2}{A}\left(\frac{Z^2}{A}\right)^2_{crit} \tag{15}$$

$$= 0.0007601 \frac{A_1^{1/3}A_2^{1/3}(A_1^{1/3}+A_2^{1/3})^2}{A}\left(\frac{Z^2}{A}\right)^2_{crit} \text{ MeV} \quad . \tag{16}$$

(Compare eqs. (30-33) in Ref. 12.) Here m is the atomic mass unit ($mc^2$ = 931.5 MeV), and we have used the Fermi-gas expression for $\rho\bar{v}$

$$\rho\bar{v} = \frac{27}{32\pi}\left(\frac{\pi}{3}\right)^{1/3} \frac{\hbar}{r_o^4} \tag{17}$$

$$= 0.79744 \times 10^{-22} \text{ MeV sec fm}^{-4} \quad , \tag{18}$$

if the value $r_o$ = 1.2249 fm, implied by Ref. 9, is adopted for illustrative purposes.

Using for $\phi$ the linear approximation given by eq. (11), we recover the formula for $E_x$ quoted as eq. (1) in Ref. 17.

The numerical calculations on which Fig. 2a is based are approximately reproduced by a choice of $x_{th}$ equal to 0.584 and the following formula for $\phi$:

$$\phi(\xi) = 5\xi + 27800\xi^7 \quad . \tag{19}$$

(The linear term by itself is accurate to 10% up to $\xi \equiv x_e - x_{th} = 0.16$, after which it rapidly becomes inadequate.) The numerical calculations of the extra-extra push $E_{xx}$ in Fig. 2b were found to be reproduced approximately by changing the argument $x_e$ to $x_m$, given by eq. (8). Thus

$$E_{xx} = E_{ch}\,\phi^2\,(x_m - x_{th}) \quad . \tag{20}$$

The result is shown in Fig. 2c for k = 1. The "cliff" in this figure is the locus where $x_m$ is a constant, i.e. $x_m = x_{cl} = 0.7$. This choice of $x_{cl}$ produces approximate agreement with Fig. 2b as regards the boundary where $E_{xx}$ exceeds $E_x$.

The above formulae, which represent the results obtained with the aid of the schematic model of Ref. 12, can be made to reproduce approximately experimental data by using the linear approximation to $\phi$ together with empirically adjusted values of the parameters $x_{th}$ and a. This leads to the following semi-empirical formulae for the extra and the extra-extra push in head-on collisions:

$$E_x = 0 \qquad \text{for} \quad x_e \leqslant x_{th} \tag{21}$$

$$E_x \approx E_{ch}\,a^2\,(x_e - x_{th})^2 = K(\zeta_e - \zeta_{th})^2 \qquad \text{for } x_e > x_{th} \tag{22}$$

and

$$E_{xx} = E_x \qquad \text{for} \quad x_m \leqslant x_{cl} \tag{23}$$

$$E_{xx} = E_{ch}\,a^2\,(x_m - x_{th})^2 = K(\zeta_m - \zeta_{th})^2 \qquad \text{for } x_m > x_{cl} \quad . \tag{24}$$

In the above, $\zeta$ is a shorthand notation for $Z^2/A$ and the constant K is given by

$$K = E_{ch}a^2/\zeta_{cr}^2 \tag{25}$$

$$= 0.0007601\,\frac{A_1^{1/3}A_2^{1/3}(A_1^{1/3}+A_2^{1/3})^2}{A}\,a^2 \text{ MeV} \quad . \tag{26}$$

For convenience, we collect together the definitions of the various symbols $\zeta$ and x in the above equations. Thus the $Z^2/A$ fissilities are given by

$$\zeta = Z^2/A \tag{27}$$

$$\zeta_e = (Z^2/A)_{eff} \quad \text{(see eq. 2)} \tag{28}$$

$$\zeta_g = \sqrt{\zeta\zeta_e} \tag{29}$$

$$\zeta_m = \zeta_g - k\zeta\left(1 - \frac{\zeta_g}{\zeta}\right)^2 \tag{30}$$

$$\zeta_{cr} = (Z^2/A)_{crit} \quad \text{(see eq. 3)} \tag{31}$$

$$\zeta_{th} = x_{th}\,\zeta_{cr} = b(1 - \kappa_s I^2) \quad , \tag{32}$$

where $$b = \frac{40\pi\gamma_o r_o^3}{3e^2}\,x_{th} = 50.883\,x_{th} = \text{"threshold coefficient" (a universal constant).} \tag{33}$$

$$\zeta_{cl} = x_{cl}\,\zeta_{cr} = c(1 - \kappa_s I^2) \quad , \tag{34}$$

where $$c = \frac{40\pi\gamma_o r_o^3}{3e^2}\,x_{cl} = 50.883\,x_{cl} = \text{"cliff coefficient" (a universal constant).} \tag{35}$$

The corresponding fissility parameters $x$, $x_e$, $x_g$, $x_m$, $x_{th}$, $x_{cl}$ are obtained by dividing by $(Z^2/A)_{crit}$, as given by eq. (3), viz.

$$x = (Z^2/A)/\zeta_{cr} \tag{36}$$

$$x_e = (Z^2/A)_{eff}/\zeta_{cr} \tag{37}$$

$$x_g = \sqrt{xx_e} \tag{38}$$

$$x_m = x_g - kx\left(1 - \frac{x_g}{x}\right)^2 \tag{39}$$

$x_{th}$, $x_{cl}$ = universal constants .

There are altogether four dimensionless parameters in eqs. (21-24), to be deduced from experiment or estimated from a dynamical model: a, $x_{th}$ (or b), $x_{cl}$ (or c), and k. Table I gives some estimates of these parameters.

Note that the final formulae for the extra and extra-extra push may be written as follows:

$$E_x = \frac{32}{2025}\left(\frac{3}{\pi}\right)^{2/3} \frac{e^4 m}{\hbar^2} \frac{A_1^{1/3}A_2^{1/3}(A_1^{1/3}+A_2^{1/3})^2}{A} a^2 \left[\left(\frac{Z^2}{A}\right)_{eff} - b(1-\kappa_s I^2)\right]^2 \quad (40)$$

$$= 0.0007601 \frac{A_1^{1/3}A_2^{1/3}(A_1^{1/3}+A_2^{1/3})^2}{A} a^2 \left[\left(\frac{Z^2}{A}\right)_{eff} - b(1-\kappa_s I^2)\right]^2 \text{ Mev} , \quad (41)$$

$$E_{xx} = 0.0007601 \frac{A_1^{1/3}A_2^{1/3}(A_1^{1/3}+A_2^{1/3})^2}{A} a^2 \left[\left(\frac{Z^2}{A}\right)_m - b(1-\kappa_s I^2)\right]^2 \text{ MeV} . \quad (42)$$

The noteworthy feature of eq. (40) is that, with the slope coefficient a and the threshold coefficient b determined empirically ($a = 12 \pm 2$, $b = 35.62 \pm 1$), eq. (40) is almost independent of any nuclear parameters. (The exception is the slight dependence on the surface symmetry energy coefficient $\kappa_s$.) In particular, the surface energy coefficient $\gamma_o$ and the radius constant parameter $r_o$ do not appear explicitly, and no assumptions about their values need be made when applying eq. (40). A similar remark applies to eq. (42), but the relevant coefficients c and k [entering in $(Z^2/A)_m$] have not, so far, been determined empirically.

The values $x_{th} = 0.723$, $a \approx 18$ in the last column of Table I were deduced from a model calculation by J. Blocki (private communication, 1981), in which the head-on collision of two equal sharp-surfaced nuclei was followed numerically using the Chaotic Regime Dynamics. (The nuclear shapes were parametrized as spheres with a hyperbolic neck, Ref. 25). The total system was assumed to be on the valley of stability [i.e. $I = 0.4A/(200+A)$] and nuclear

parameters were used according to which $(Z^2/A)_{crit} = 50.805\ (1 - 2.204I^2)$. Using this model, Blocki found that, starting with zero kinetic energy at contact, a system with mass number A = 209 would fuse, but for A = 213 it would reseparate, having failed to overcome the saddle-point pass. Taking $A \approx 211$ ( Z = 83.8353) as an estimate of the mass number corresponding to the threshold condition, one finds $x_{th} = [(83.8353)^2/211]/50.805(1-2.204I^2) = 0.723$, and $b = 50.805\ x_{th} = 36.73$.

In another set of numerical studies, Blocki found that a system with A = 242 (Z = 94.5005) needed about 40 MeV of extra push over the contact configuration to fuse. The effective fissility of this system is $x_e = 0.8122$. Using eq. (22) it follows that

$$a \approx \sqrt{\frac{40\ \text{MeV}}{E_{ch}}} \cdot (x_e - x_{th})^{-1} \approx 18.0 \quad . \tag{43}$$

Feldmeier (Ref. 26 and private communication) has pointed out that when the extra push is 40 MeV (and $x_e - x_{th}$ is of the order of 0.1) the nonlinearity in the dependence of $\sqrt{E_x}$ on $(x_e - x_{th})$ is appreciable and that if allowance were made for this, the value of a deduced from Blocki's calculation for A = 242 would be reduced.

Figures 3 and 4 illustrate eqs. (21-24) for systems composed of two pieces with atomic numbers $Z_1$, $Z_2$, each of which is assumed to be on the valley of beta stability, as given by Green's formula, $N-Z = 0.4A^2/(200+A)$. This makes the figures more nearly relevant to actual experimental situations than Fig. 2, where the total system was assumed to be on the valley of stability, and the implied projectiles have often quite unrealistic values of the neutron excess.

In constructing Figs. 3 and 4 we used the empirical values $x_{th} = 0.70$, a = 12 and the illustrative values k = 1, $x_{cl} = 0.84$. This value of $x_{cl}$

follows from rescaling the schematic model value $x_{c1} = 0.70$ by the factor 1.2, which is the ratio of the empirical to the schematic value of $x_{th}$ (i.e. 0.70: 0.584 = 1.20). The values k = 1, $x_{c1} = 0.84$ are also consistent with experimental indications discussed in the last paragraph of Sec. 3, which suggest $0.84 \lesssim x_{c1} \lesssim 0.86(?)$. It cannot be stressed too emphatically, however, that the true values of k and $x_{c1}$ are simply not known at the present time. On the contrary, the schematic model is known to be quite inadequate for quantitative predictions and the experimental indications concerning an upper limit on $x_{c1}$ are marginal at best and could be misleading. Hence the actual MeV values of the extra-extra push in Fig. 4, as well as the location of the cliff, are meant as qualitative illustrations only.

As in Refs. 17,20 we may generalize the expressions for $E_x$ to the case when an angular momentum L is present, by adding to the Coulomb potential an effective centrifugal potential, proportional to $L^2$ divided by twice an effective moment of inertia or, what comes to the same thing, a centrifugal potential equal to the square of an effective angular momentum, $(fL)^2$, divided by twice the standard moment of inertia $M_r(R_1+R_2)^2$, appropriate for approaching spheres just before contact. Here f is an "effective angular momentum fraction" (Ref. 17). The generalized formula for $E_x$ may then be written as follows:

$$E_x = 0 \qquad \text{for } \zeta_e(\ell) \leqslant \zeta_{th} \tag{44}$$

$$E_x = K[\zeta_e(\ell) - \zeta_{th}]^2 \qquad \text{for } \zeta_e(\ell) > \zeta_{th} \quad , \tag{45}$$

where

$$\zeta_e(\ell) = \zeta_e + (f\ell/\ell_{ch})^2 \quad . \tag{46}$$

Here $\zeta_e(\ell)$ is a generalized effective fissility and $\ell/\ell_{ch}$ [equal to $(L/\hbar)/(L_{ch}/\hbar)$] is the total angular momentum quantum number in units of a characteristic angular momentum quantum number of the system, $\ell_{ch}$, given by

$$\ell_{ch} = \frac{e\sqrt{mr_o}}{2\hbar} \frac{A_1^{2/3}A_2^{2/3}\left(A_1^{1/3}+A_2^{1/3}\right)}{\sqrt{A}} \tag{47}$$

$$= 0.10270 \frac{A_1^{2/3}A_2^{2/3}(A_1^{1/3}+A_2^{1/3})}{\sqrt{A}} \quad . \tag{48}$$

An empirical value of the angular momentum fraction, $f \approx 3/4 \pm 10\%$, was deduced in Ref. 17. (It appears to be consistent with the recent theoretical estimates in Ref. 28, $f \approx 0.85 \pm 0.02$.)

The problem of generalizing the extra-extra push to include angular momentum is more difficult, since a simple trading of centrifugal for electrostatic forces becomes questionable in the mononuclear regime. In particular, when the nuclear shape approaches the sphere, there is a qualitative difference between the electric potential, which is stationary for the sphere, and the centrifugal potential, which is not. The use of a <u>constant</u> angular momentum fraction is thus certainly not valid. An angular momentum <u>function</u> that is made to depend on the fissility parameter x might have more validity, and we are trying the following prescription. We first define a generalized, angular-momentum dependent fissility $x(\ell)$ in the mononuclear regime by

$$x(\ell) = x + \eta(x)y \quad ,$$

where $\eta(x)$ is a function to be determined presently and y is the standard rotational parameter of fission theory (Ref. 29), proportional to the square of the angular momentum, and given by

$$y \equiv \frac{\text{(Rotational energy of rigid sphere)}}{\text{(Surface energy of sphere)}} \tag{49}$$

$$= \frac{L^2 / \frac{4}{5}MR^2}{4\pi R^2 \gamma} \tag{50}$$

$$= \frac{1.9407}{1-1.7826I^2} \frac{\ell^2}{A^{7/3}} \quad . \tag{51}$$

The function $\eta(x)$ is now determined by the requirement that the fission barrier of the rotating system should vanish at the correct value of the angular momentum. Thus, when the rotational parameter y reaches the critical value (denoted by $y_{II}(x)$ in Ref. 29), at which the fission barrier of a rotating liquid drop (characterized by a fissility parameter x) vanishes, the generalized fissility parameter $x(\ell)$ should reach unity (the critical value for the vanishing of the barrier of a nonrotating drop). It follows that

$$\eta(x) = \frac{1-x}{y_{II}(x)} \quad . \tag{52}$$

The numerical calculations of $y_{II}(x)$ from Ref. 29 may be represented by the analytical formulae given in the Appendix and these were used to prepare Table II for $\eta(x)$. From the generalized fissility parameter $x(\ell)$ obtained in this way we may derive the following formula for the generalized fissility $\zeta(\ell)$ in the mononuclear regime:

$$\zeta(\ell) = x(\ell)\zeta_{cr}$$

$$= \zeta + \eta(x) \frac{L^2 / \frac{4}{5}MR^2}{4\pi R^2 \gamma} \frac{40\pi r_o^3 \gamma}{3e^2} \tag{53}$$

$$= \zeta + \eta(x) \, (\ell/\ell_o)^2 \quad , \tag{54}$$

where

$$\ell_o = \frac{\sqrt{6}}{5} \frac{e\sqrt{mr_o}}{\hbar} A^{7/6} = 0.10063A^{7/6} \quad . \tag{55}$$

One way to generalize the mean fissility $\zeta_m$ for angular momentum would be to use eq. (30), but with $\zeta_e$ replaced by $\zeta_e(\ell)$ [eq. (46)] and $\zeta$ replaced by $\zeta(\ell)$ [eq. (54)]. An approximately equivalent scheme that is more convenient for subsequent cross-section calculations defines $\zeta_m(\ell)$ as $\zeta_m$ augmented by the geometric mean of the $\ell$-dependent terms in eqs. (46) and (54). Thus

$$\zeta_m(\ell) \equiv \zeta_m + \sqrt{(f\ell/\ell_{ch})^2 \cdot \eta(x)(\ell/\ell_o)^2} \quad .$$

$$= \zeta_m + (f_m\ell/\ell_{ch})^2 \quad . \tag{56}$$

Here $f_m$ is a "mean angular momentum function", given by

$$f_m = [\eta(x)]^{1/4} \sqrt{f\ell_{ch}/\ell_o} \tag{57}$$

$$= \sqrt{f}\ [\eta(x)]^{1/4} \left(\frac{25}{24}\right)^{1/4} \frac{A_1^{1/3}A_2^{1/3}(A_1^{1/3}+A_2^{1/3})^{1/2}}{A^{5/6}} \tag{58}$$

$$= \sqrt{f}\ [\eta(x)]^{1/4} \left(\frac{25}{24}\right)^{1/4} \frac{\theta(1+\theta)^{1/2}}{(1+\theta^3)^{5/6}} \quad , \tag{59}$$

where $\theta = (A_1/A_2)^{1/3}$ .

The corresponding formula for the generalized mean fissility parameter $x_m(\ell)$ is

$$x_m(\ell) = x_m + (f_m\ell/\ell_{ch})^2\ \zeta_{cr} \quad . \tag{60}$$

The generalized formula for the extra-extra push may now be written as

$$E_{xx} = E_x \qquad \text{for } \zeta_m(\ell) \leqslant \zeta_{cl} \tag{61}$$

$$E_{xx} = K[\zeta_m(\ell) - \zeta_{th}]^2 \qquad \text{for } \zeta_m(\ell) > \zeta_{cl} \quad . \tag{62}$$

Note that, since $f_m$ is given uniquely in terms of f, no new adjustable parameters have been introduced in our scheme of estimating the extra-extra push in the presence of angular momentum. This is just as well, since this aspect of the theory is so uncertain that it would be foolish to hide its anticipated shortcomings by the adjustment of an arbitrary and possibly unphysical parameter.

## 3. Cross Sections

According to the Extra Push Theorem of Ref. 17, conservation of energy and angular momentum leads to the following relation between the center-of-mass energy E and the cross section $\sigma$ (equal to $\pi b^2$, where b is the largest contributing impact parameter) for a process that demands for its inception an extra radial injection energy containing a contribution from the centrifugal repulsion, assumed to be proportional to the square of the angular momentum:

$$\sqrt{E - B - \frac{\sigma E}{\pi r^2}} = \alpha + \beta \frac{\sigma E}{\pi r^2} + \ldots \quad . \tag{63}$$

Here B is the potential energy and r the center separation at contact. The quantities $\alpha,\beta$ are constants for a given colliding system. Eq. (63) follows by inspection from the (square root of) the energy conservation equation: the left-hand side is the square root of the energy available for radial motion at contact (because $\sigma E/\pi r^2$, equal to $b^2E/r^2$, equal to $L^2/2M_r r^2$, is the orbital energy) and is thus equal to the square root of the extra or extra-extra push. The right-hand side is a way of writing this quantity (proportional to the extra injection velocity at contact) as consisting of an L-independent part and a centrifugal part, proportional to $L^2$ ($\sigma E/\pi r^2$ is proportional to $L^2$, see above). If eqs. (45,62) are used for $E_x$ and $E_{xx}$, the constants $\alpha$ and $\beta$ are found to be given by

$$\alpha_x = \sqrt{K}\,(\zeta_e - \zeta_{th}) \quad , \qquad \alpha_{xx} = \sqrt{K}\,(\zeta_m - \zeta_{th}) \quad , \tag{64}$$

$$\beta_x = \frac{8\sqrt{K}}{e^2/r_o}\,\frac{f^2}{A_1^{1/3}A_2^{1/3}} \quad , \qquad \beta_{xx} = \frac{8\sqrt{K}}{e^2/r_o}\,\frac{f_m^2}{A_1^{1/3}A_2^{1/3}} \quad , \tag{65}$$

the suffixes x or xx referring to the extra or extra-extra push, respectively.

The solution of the quadratic equation (63) is

$$\sigma = \frac{\pi r^2}{E}\left[\sqrt{\left(\frac{\alpha\beta+\frac{1}{2}}{\beta^2}\right)^2 - \left(\frac{\alpha^2+B-E}{\beta^2}\right)} - \left(\frac{\alpha\beta+\frac{1}{2}}{\beta^2}\right)\right] \tag{66}$$

and gives explicitly the energy-dependence of the cross section for a process requiring for its initiation a certain additional radial energy over the interaction barrier.

Figure 5a illustrates the nature of the excitation functions predicted by eq. (66). The solid curve is the cut-off value of $\pi b^2$ above which the two idealized nuclei do not touch, as given by the standard formula

$$\sigma = \pi b^2 = \pi r^2\,(1 - \frac{B}{E}) \quad , \tag{67}$$

obtained by setting to zero the right-hand side of eq. (63) (no extra push). For impact parameters b above the solid curve, the collisions are dominated by elastic scattering. (In a more refined model that takes into account the diffuseness of the nuclear surfaces, quasi-elastic events would appear for b values around the solid curve.) Thus the solid curve gives approximately the reaction cross section. The dashed curve in Fig. 5a gives the value of $\pi b^2$ below which the extra push in the radial direction has been exceeded, the conditional saddle has been overcome, and fusion has taken place in the sense of the formation of a mononucleus. The area between the solid and dashed curves corresponds, therefore, to dinucleus (deep-inelastic) reactions. The

dotted curve corresponds to the locus of impact parameters above which the schematic model (with nominal parameters) suggests that the spherical shape would not be attained (because of the entrance-channel, extra-extra push limitation) and a mononucleus (fast-fission) reaction would be expected. The dotted curve was drawn using eqs. (61,62) for the extra-extra push, with $k = 1$, $x_{c1} = 0.85$, and $f_m$ given by eq. (59). (The value of $x_{c1}$ is a little larger than the 0.84 used in drawing Fig. 4.) Since none of the relevant quantities, $k$, $x_{c1}$, $f_m$, is well known, the dotted curve is shown for illustrative purposes only, and it should not be taken as a quantitative prediction of the theory. The schematic model suggests that below the dotted curve the vicinity of the spherical shape might be attained. This still does not mean that a compound nucleus would be formed since, for this to be the case, there should be present a finite barrier against redisintegration. In the example illustrated in Fig. 5a, this might actually not be the case at high energies: the dot-dashed curve shows the locus of impact parameters along which the fission barrier, calculated according to the rotating liquid drop model has vanished (see Appendix). Thus <u>all</u> of the region between the dashed and dot-dashed curves would correspond to mononucleus (fast-fission) reactions. Below the dot-dashed curve a finite fission barrier begins to grow, increasing in proportion to the distance below the critical locus (labeled $B_f = 0$). Reactions captured inside the potential-energy hollow defined by this barrier will not disintegrate until after a certain time delay, which the system requires to find its way out of the hollow. According to the statistical theory of rate processes, the lengthening of the fission lifetime is expected to be, roughly, by a factor involving the exponential of the fission barrier divided by the relevant nuclear temperature at the saddle point for fission. For finite temperatures the fission lifetimes are, therefore, not expected to change

suddenly as the reaction moves into the region below the dot-dashed curve. In fact, the transition should be quite gradual. When, however, the fission barrier has grown sufficiently, the lengthening of the lifetime should become drastic (exponentially) and may, in typical cases, amount to several powers of ten if the temperature is a fraction of an MeV, but only one or two powers of ten (or less) for temperatures of several MeV. The decay of the compound nucleus by fission, after the above time delay, is expected to dominate when the fission barrier is less than the barrier against particle emission, most often (but not exclusively) neutron emission. The triple dot-dashed curve in Fig. 5a shows the locus along which the fission barrier of the rotating liquid drop has reached the value $B_n$, the neutron binding energy. Below about this locus the decay of the compound nuclus should be dominated by particle (neutron) evaporation, leading to evaporation residues rather than fission fragments as the final products of the reaction. The lifetimes of these evaporation residues (after further deexcitation) may be very long, being governed by the relevant alpha decay or spontaneous-fission lifetimes. Illustrative orders of magnitude of the different characteristic lifetimes are noted on the right of Fig. 5a. The abscissa itself in Fig. 5a corresponds to the locus of zero impact parameters (head-on collisions), where the fission barrier has attained its maximum height, coresponding to a system with no angular momentum, as indicated by the label $B_f(L = 0)$.

The theoretical curves in Fig. 5a (representing the reaction $^{116}Sn + ^{35}Cl$, with a combined atomic number Z = 67) were constructed using the formulae explained above (and detailed in the Appendix), using the following values of the parameters: $x_{th} = 0.70$, a = 12, f = 3/4. (These are the values deduced from a fit to the fusion data of Ref. 20, involving heavier systems in the atomic number range Z = 94-110.) A comparison with

experimental data (Ref. 21) is shown in Fig. 5b. The triangles are measured evaporation-residue cross sections, and the circles are sums of evaporation residues and fission-like events. An approximate correspondence with the triple dot-dashed and dashed curves is evident. Figure 5c makes a similar comparison with the slightly lighter system $^{109}Ag + ^{40}Ar$ (Z = 65) and Fig. 5d with $^{141}Pr + ^{35}Cl$ (Z = 76). Considering the uncertainties of the measurements there does not appear to be evidence for a serious disagreement at this stage, but the fact that the fusion cross sections (the circled points) are systematically higher than the calculated dashed curves may be significant. (Compare Ref. 21.)

Figures 6a-6g provide essentially the same confrontation of theory and experiment as Refs. 17,20, except that the calculated curves are now based on using the parameter $x_{th} = 0.70$ rather than $(Z^2/A)_{th} = 33$ to define the threshold fissility. Note the small three-digit numbers appearing above the dashed curves in Figs. 5, 6, and 8. They give the values of $x_e(\ell)$ along these curves as function of bombarding energy. At the critical energy where the dashed curve peels off from the solid curve the corresponding label would be 0.70, the value of $x_{th}$. We see that in the energy range displayed, the values of $x_e(\ell)$ soon exceed 0.8. Since (for symmetric systems) $x \approx 0.8$ marks the point where the saddle-point shape loses its neck constriction (and becomes convex everywhere for $x \gtrsim 0.8$), one might have expected that the physical significance of the conditional saddle-point shape would be lost beyond $x_e(\ell) \approx 0.8$. The distinction between deep-inelastic and fast-fission reactions should then be more and more difficult to maintain. (Thus the dashed curves ought to have been made to fade out towards the right, so that the deep-inelastic and fast-fission reactions would merge at high energies.) Note also that for the heavier systems in Fig. 6 the predicted need for an

extra-extra push could be playing an increasingly important role. For example, in the case of $^{208}Pb + ^{50}Ti$, the entrance-channel limitation on compound-nucleus formation, related to the cliff in Fig. 4 and resulting in the dotted curve in Fig. 5d, is comparable with the limit imposed by the vanishing of the fission barrier for a rotating liquid drop (dot-dashed curve). In Fig. 5e the dotted curve actually dips significantly below the dot-dashed curve and in Figs. 5f and 5g there is finally a need for an extra-extra push to form a compound nucleus even in head-on collisions. Two things should, however, be kept in mind. First, the location of the dotted curves depends on the parameters $x_{cl}$ and k and the function $f_m$, whose values are unknown. (The values $x_{cl} = 0.85$, $k = 1$, chosen for purposes of illustration, should not be allowed to acquire the status of a theoretical prediction.) Second, by the time the dotted curves in Figs. 5d-5g become a more serious limitation on compound-nucleus formation than the dot-dashed curves, the fission barriers, even for head-on collisions, are only a fraction of an MeV. Thus, the extra-extra push entrance-channel limitation would be almost academic. The entrance-channel limitation might conceivably be more relevant when the compound nucleus is stabilized by a shell effect. In such cases the barrier against fission might be several MeV but the requirement of an extra-extra push might prevent the system from reaching the vicinity of the spherical shape, where the shell effect would have a chance to manifest itself.

A confrontation of the present theory with experiments on compound nucleus formation cross sections is becoming possible through the analysis of evaporation residue measurements. A particularly relevant set of experimental "effective barriers" for the formation of compound nuclei has been presented in Ref. 30. These are barriers that would have to be inserted in conventional calculations of evaporation-residue cross sections in order to reproduce the

observed cross sections for various (xn) reactions following the collision of two nuclei. By comparing such barriers with standard interaction barriers (either measured directly or calculated by an adequate semi-empirical procedure fitted to measurements throughout the lighter part of the periodic table) one may look for anomalies (in the case of heavy reacting systems) that would signal the need for an extra or extra-extra push. Table III, based on Refs. 30,32, lists six estimated effective barriers and two lower limits. These are compared with interaction barriers estimated semi-empirically. (These estimates were made by lowering by 4% theoretical barriers obtained by combing the nuclear Proximity Potential with the Coulomb interaction between two (point) charges; see Ref. 31.) The differences between experimental and theoretical estimates are plotted in Fig. 7. These are compared with the formula for $E_x$, eqs. (21,22). The experimental points can hardly be claimed to determine a smooth trend with which the theory could be compared and the uncertainties are so large that it is difficult to say if there is agreement or disagreement. The lower limits in the case of the $^{86}Kr + ^{160}Gd$ and $^{110}Pd + ^{136}Xe$ reactions suggest that a significant anomaly is present at least in those two cases, which would translate into an extra push in excess of 20 MeV. The calculated curve, based on a threshold parameter $x_{th}$ equal to 0.70 (corresponding to an average value of $(Z^2/A)_{th}$ of about 33.5 for the set of eight reactions in Fig. 7) does a respectable job of passing through the scattered data points. To pass through the $^{86}Kr + ^{123}Sb$ point, $(Z^2/A)_{th}$ would have to be lowered by about 1.5 unit. If, for some reason, the $^{86}Kr + ^{123}Sb$ point were to be disregarded, an <u>increase</u> of $(Z^2/A)_{th}$ by one unit would be indicated. (This corresponds to an increase of $x_{th}$ by 0.02.) An increase by more than one unit would begin to violate the lower limits set by $^{86}Kr + ^{160}Gd$ and $^{76}Ge + ^{170}Er$, and an increase by two units would also begin to violate the limit set by $^{110}Pd + ^{136}Xe$.

The data are consistent with a position of the cliff near to or above the $^{86}Kr + ^{160}Gd$ point, for which the value of $\zeta_g$ is 39.9 and the value of $x_m$ is 0.835. The $^{209}Bi + ^{54}Cr$ reaction with $x_m = 0.829$ also appears to be below the cliff; see the following section. Thus we deduce tentatively that $x_{cl} \gtrsim 0.84$, $(Z^2/A)_{cl} \gtrsim 40$ in round numbers. Experimental evidence allowing an estimate of an upper limit for $x_{cl}$ is even more uncertain, but one might argue as follows. It may be expected that angular distributions of the fission fragments from compound nucleus reactions will be forward-backward symmetric, because the compound system makes many revolutions as it decays. Conversely, a fast-fission reaction may take place in a time less than required for one-half revolution and could, therefore, result in an angular distribution intermediate between the compound-nucleus type and the strongly focused, deep-inelastic type. As an example, the reaction $^{50}Ti + ^{208}Pb$ with $x_m = 0.79$ is found to be of the compound nucleus type, when the bombarding energy is close to the barrier and the contributing $\ell$-values are below 40 $\hbar$, Ref. 20. On the other hand, the $^{56}Fe + ^{208}Pb$ reaction with $x_m = 0.858$ $((Z^2/A))_m = 41.1)$ gives rise to forward-backward asymmetric angular distributions of the fast type at all bombarding energies including the lowest, where the maximum contributing $\ell$-value is about 30 $\hbar$, Ref. 33. From these two experiments one might estimate that $x_{cl}$ should lie between 0.79 and 0.86. It should be stressed that this interpretation of the two experiments is not unambiguous. The noncompound features found with the $^{56}Fe + ^{208}Pb$ reactions could be due to interference from tails of the deep inelastic angular and mass distributions, thus obscuring an underlying reaction with perfect compound equilibrium properties. (Such interferences would be less pronounced in the case of the $^{50}Ti + ^{208}Pb$ reaction, because the symmetric mass yields are higher here.) Combining the tentative lower

limit $x_{cl} \gtrsim 0.84$ with the hypothetical upper limit $x_{cl} \lesssim 0.86$ we decided to use $x_{cl} = 0.85$ as an illustrative value when preparing Figs. 5,6,8.

## 4. Superheavy Element Reactions

Figure 8a illustrates the application of the present theory to the reaction $^{209}Bi + ^{54}Cr$, which has recently led to the unambiguous identification of element 107 (Refs. 34,35). Figure 8b illustrates the reaction $^{248}Cm + ^{48}Ca$, which is a candidate for making a superheavy nucleus with the neutron number sufficiently close to the anticipated magic number N = 184 to make it detectable--perhaps--with available experimental techniques. (In what follows, whenever we quote predicted shell effects, barriers, and half-lives for superheavy nuclei, we will use, for the sake of definiteness, Figs. 4, 5a, and 8 of Ref. 36. We treat the resulting numbers as nominal reference values useful, we hope, as a guide for estimating relative magnitudes. The absolute magnitudes of any predictions concerning superheavy elements we regard as still very uncertain.) In the calculations in Fig. 8a the extra push has just become a factor in head-on collisions, suggesting that the experimental center-of-mass bombarding energies of 208.1 MeV and 212.4 MeV (indicated by the arrows) may be only marginally sufficient to induce fusion. (In this connection see the discussion in Section VI of Ref. 17.) The extra-extra push (calculated using $x_{cl} = 0.85$, $k = 1$) is about to become an additional limiting feature in head-on collisions, but it is important to bear in mind the caveats, stressed previously, about taking at face value this feature of the theory. However, the comparison of the two reactions $^{209}Bi + ^{54}Cr$ and $^{248}Cm + ^{48}Ca$ brings out the interesting fact that, as regards macroscopic entrance channel limitations, the two cases are fairly similar, both as regards the extra and the extra-extra push. This is related to the fact that the two scaling

parameters $x_e$ and $x_m$, or $(Z^2/A)_{eff}$ and $(Z^2/A)_g$, are quite similar in the two cases. In particular, since $x_e$ is, in fact, a little lower for $^{248}Cm + ^{48}Ca$ than for $^{209}Bi + ^{54}Cr$, and the latter is known to have led to a compound nucleus, <u>it is fairly safe to expect that in the case of $^{248}Cm + ^{48}Ca$ fusion will occur</u>, in the sense of the overcoming of the conditional saddle and the formation of a mononucleus. The formation of a compound nucleus is, however, much more problematic; even if there is a sufficiently pronounced shell effect to make element $^{296}116$ potentially stable against fission, the fission saddle point is expected in this case to be more compact than in the case of element $^{263}107$ (the outcome of the $^{209}Bi + ^{54}Cr$ reaction). This is because the ground state is expected to be spherical for element 116 but deformed for element 107. Hence, the formation of the 107 compound nucleus could have been favoured by a relatively deformed fission saddle point shape, a bonus that is likely to be absent in the case of $^{248}Cm + ^{48}Ca$. A similar phenomenon might be contributing to the mysterious failure of the spherical N = 126 shell to enhance the survival, as evaporation residues, of the light actinides with spherical equilibrium shapes (such as $^{216}Th$) (Refs. 37,38,39). The mystery is that the heavier actinides, with their deformed equilibrium shapes, <u>do</u> show the anticipated enhanced survival associated with the (deformed) shell effect. Since, for the spherical actinides, the shell effect operates only in the vicinity of the compact spherical shape, it is possible that the dynamical fusion trajectories have only a very poor chance to become aware of the associated potential-energy hollow, and the compound-nucleus formation probability is consequently relatively low. (An extra-extra push would, however inefficiently, help to direct the trajectory toward the hollow.) The riddle of the impotence of the spherical N = 126 shell is a dark cloud on the

superheavy element horizon. It remains to be seen whether the suggested relation to the extra-extra push phenomenon is a contributing factor in the explanation. However that may turn out, it is clear that, when the saddle point shapes are affected by shell effects, the macroscopic parameters $x_m$ or $(Z^2/A)_g$ are no longer reliable scaling parameters for comparing different reactions.

Keeping these reservations in mind, we present in Table IV a comparison of different characteristics of three superheavy reactions with the "calibrating" reaction $^{209}Bi + ^{54}Cr$, viz.

1. $^{209}Bi_{83} + ^{54}Cr_{24} = ^{263}107$ (N = 156)
2. $^{248}Cm_{96} + ^{48}Ca_{20} = ^{296}116$ (N = 180)
3. $^{252}Cf_{98} + ^{48}Ca_{20} = ^{300}118$ (N = 182)
4. $^{254}Es_{99} + ^{48}Ca_{20} = ^{302}119$ (N = 183)

We note that all three superheavy reactions have similar values of $(Z^2/A)_{eff}$, so in all cases one may reasonably hope for the formation of a mononucleus when the bombarding energy is close to the estimated interaction barrier. At these energies the deexcitation of the compound nucleus would most likely proceed by the emission of two or three neutrons, and in this respect all three reactions are inferior to the $^{209}Bi + ^{54}Cr$ reaction, which, with about 9 MeV less excitation, can result in the emission of only one or two neutrons. However, by using a center-of-mass energy only 4.66 MeV below the nominal barrier for $^{248}Cm + ^{48}Ca$ in Table IV, the estimated excitation energy of the compound nucleus would be 20.95 MeV, and with 9.54 MeV below the nominal barrier the excitation would be 16.16 MeV, which are the estimated excitations in the $^{209}Bi + ^{54}Cr$ reactions at the energies used in

the 107 experiment (4.95 MeV/amu and 4.85 MeV/amu). Since, with these excitations, a 1n reaction was observed, and since subnominal-barrier cross sections ought to be enhanced more strongly in the case of softer and deformed targets like $^{248}Cm$, $^{252}Cf$, $^{254}Es$, the possibility of 1n reactions of the type $^{248}Cm + ^{48}Ca = ^{295}116 + n$, $^{252}Cf + ^{48}Ca = ^{299}118 + n$, $^{254}Es + ^{48}Ca = ^{301}119 + n$, would appear to be well worth exploring. (This has been brought to our attention by discussions with P. Armbruster and his colleagues at GSI; see Refs. (34,35)). The estimated fission barriers for the resulting three superheavy nuclei after neutron emission would be higher by about 3/4 MeV, the estimated even-even fission lifetimes would be longer by about three orders of magnitude, and, in addition, all three reactions might now benefit from an odd-A lifetime enhancement. The last three lines in Table IV illustrate these estimates. Finally, we should note that if the 1n superheavy element reactions turn out to be a reality, the reaction $^{250}Cm + ^{48}Ca = ^{297}116 + n$ would lead to an element for which the estimated fission lifetime is $10^{-7}$ y and the alpha lifetime is $10^{-6}$ y (plus an odd-A enhancement). Allowing for an uncertainty in the lifetime estimates of several powers of 10 either way, the range of possibilities includes readily detectable activities in the millisecond range, to a reasonably stable element, susceptible to a range of chemical studies.

If the prediction of a closed neutron shell at N = 184 is correct, then, of the three superheavy reactions in Table IV, the case of $^{254}Es + ^{48}Ca$, with N = 183, offers the advantages of the highest fission barrier and the longest spontaneous fission lifetimes. Since, after the emission of two neutrons, one would be dealing with an odd-odd nucleus, an extra bonus in decay hindrance factors might be expected, which could be of decisive importance if the detection is lifetime limited rather than cross-section limited.

The "side-step" or charge-adjustment reactions in Table IV refer to a process where the charges on the two parts of the dinuclear system are readjusted during the assault on the conditional saddle (i.e. a proton from the projectile changes places with a neutron from the target, at fixed mass numbers of the two pieces). In all four reactions such an exchange is not favoured energetically, but the cost is only about 1 and 1½ MeV for the systems $^{209}Bi + ^{54}Cr$ and $^{254}Es + ^{48}Ca$, respectively. Since such a charge adjustment lowers somewhat the value of $(Z^2/A)_{eff}$, it is possible that, after paying the price of 1 or 1½ MeV for the readjustment, the resulting system gains sufficiently in fusion probability to make such a reaction a dominant path toward compound-nucleus formation. Even the cost of a double charge adjustment may not be prohibitive. If that were so, then, in the case of $^{254}Es + ^{48}Ca$, one would be assaulting the conditional barrier with an effective super-exotic reaction equivalent to $^{254}Md + ^{48}Ar$!

This possibility illustrates the general feature that attempts to make heavy or superheavy elements are likely to rely not on average or most probable reaction characteristics but on tails--perhaps extreme tails--of multi-dimensional probability distributions in several reaction parameters. Since the theory of nuclear dynamics described in the present paper is not only approximate but deals manifestly with estimates of average behavior, care should be exercised in applying such estimates to the question of the production of heavy or superheavy elements. For example, in the case of Fig. 8(a), it would be unwise to conclude that, because, after lengthy irradiations, three atoms of element 107 were produced at each of the two energies indicated by the arrows, the result contradicts the theoretical estimate that the most probable reaction trajectory would need several MeV of additional energy (plus or minus a few MeV) to overcome the conditional saddle

point. On the contrary, if a given reaction appears to be only marginally above or below a limit set by our approximate, average theory, there is reason for optimism, since it is likely that at least the tails, if not the bulk of the trajectory distributions, will succeed in achieving the desired reaction.

## 5. Summary and Conclusions

This paper was concerned with exploring some of the consequences of the Chaotic Regime Nuclear Dynamics. The schematic algebraic model of Ref. 12 was used as a guide in suggesting the mathematical structure of certain aspects of nucleus-nucleus collisions. An attempt was made to disentangle this general algebraic structure from the numerical parameters that the schematic model could not be expected to predict correctly and to determine some of those parameters from comparisons with experiments. Even though the confrontations of theory and experiment are, at this stage, not discouraging, it should be stressed that there are many serious uncertainties in the situation. First, the Chaotic Regime Dynamics is only an extreme idealization, and it is an open question how well it should apply to collisions between nuclei, where symmetries of various kinds lead one to expect deviations from the chaotic regime. Second, even within the framework of the Chaotic Regime Dynamics, the guiding model of two sharp-surfaced spheres connected by a portion of a cone is so highly schematic that one ought to have serious reservations about even its qualitative validity in certain cases. Furthermore, the mocking up of the subtle centrifugal and Coriolis effects associated with the presence of angular momentum by an increase of the electric repulsion is at a very primitive level, in particular in the mononuclear regime. Finally, the presence of several adjustable parameters in a theory is always a danger and, although often unavoidable in the initial analysis of a complex process, it

may encourage misleading conclusions; it certainly decreases the clarity of the lessons to be extracted from the confrontation of theory and experiment.

Some of the tentative conclusions of this work may be stated as follows:

1. The predicted structure of the excitation functions for the fusion of two nuclei seems consistent with the limited data available so far. A quantitative fit appears possible if three parameters are adjusted.

2. Of the three fitted parameters, the first two, $x_{th}$ and f, come out to be reasonably close to theoretical estimates (based on a dynamic model of a sharp-surfaced nucleus with one-body dissipation) and the third, a, may or may not be consistent with that model.

3. The tentative data on compound nucleus residues is not inconsistent with the extra push deduced from fusion data, but the comparison is subject to many uncertainties. There is up to now no evidence confirming directly the existence of a "cliff", where the extra-extra push is supposed to exceed rapidly the extra push, and no experimental determination of the parameters locating this cliff is available.

4. The experimental observation of element 107 in the reaction $^{209}Bi + ^{54}Cr$, taken in conjunction with the scaling parameter $x_{eff}$ or $(Z^2/A)_{eff}$, suggests that in superheavy reactions of the type $^{248}Cm + ^{48}Ca$, $^{252}Cf + ^{48}Ca$, $^{254}Es + ^{48}Ca$, it should be possible to overcome the second hurdle (the conditional saddle) using bombarding energies close to the interaction barrier. The overcoming of the true saddle and the formation of a compound nucleus is more problematic. Without being able to make quantitative predictions, the theory suggests that even the most

asymmetric available superheavy reactions may be close to a limiting obstacle (the cliff) and that one may have to rely on tails of probability distributions in order to make a compound nucleus. As a result, success or failure in the assault on the predicted island of stability may depend on squeezing out the last bit of asymmetry, neutron excess, and detection speed and sensitivity from the experimental techniques.

To sum up, it is clear from the above considerations that we are only at the beginning of our quest to develop and confirm experimentally a theory of macroscopic nuclear shape evolutions in general and to delineate the validity of the Chaotic Regime Dynamics in particular.

Acknowledgements

The authors are happy to acknowledge the close collaborations and many discussions with members of the experimental groups of R. Bock and P. Armbruster at GSI, which provided the principal stimulus for these investigations. In particular, we would like to thank P. Armbruster, A. Gobbi, H. Gäggler, K.-H. Schmidt, and W. Reisdorf, as well as M. Blann at the Lawrence Livermore Laboratory, for many insights into the physics of nucleus-nucleus collisions. We would like to thank J. Blocki, H. Esbensen, G. Fai, and H. Feldmeier for sharing with us the results of their theoretical studies.

This work was supported by the Director, Office of Energy Research, Division of Nuclear Physics of the Office of High Energy and Nuclear Physics of the U.S. Department of Energy under Contract DE-AC03-76SF00098 and by the Danish Natural Sciences Council.

## APPENDIX. Rectilinear Cross Section Plots

The cross section plots in Figs. 5, 6 and 8 are either pieces of rectangular hyperbolas (e.g. the solid curves, given by eq. (67)) or more complicated curves (e.g. the dashed curve, given by eq. (66)). It turns out that all the curves may be transformed into segments of straight lines by a simple change of variables. Thus, instead of a plot of $\sigma$ vs E, consider a plot of $Y(E,\sigma)$ vs $X(E,\sigma)$, where

$$Y \equiv \frac{\sigma E}{\pi r^2} \text{ is the "energy-weighted reduced cross section" of Ref. 17, equal to the orbital energy at contact,} \tag{A1}$$

and

$$X \equiv \sqrt{E - B - \frac{\sigma E}{\pi r^2}} \text{ is the square root of the "cross section defect" of Ref. 17, equal to the square root of the radial energy } E_r \text{ at contact.} \tag{A2}$$

It is clear that eq. (67) for the reaction cross section corresponds to $X = 0$ and is, therefore, given by the vertical Y-axis in Fig. 9. Equation (63), defining the limit to fusion set by the extra push, is given by

$$X = \alpha_x + \beta_x Y \quad , \tag{A3}$$

which is a portion of a straight line with slope $1/\beta_x$ and intercept $-\alpha_x/\beta_x$. The limit associated with the extra-extra push above the cliff is similarly a portion of the straight line

$$X = \alpha_{xx} + \beta_{xx} Y \quad . \tag{A4}$$

The cliff itself corresponds to a critical angular momentum obtained by solving the equation $\zeta_m(\ell) = \zeta_{cl}$ for $\ell$ (see eq. (61)). Now a constant angular momentum corresponds to a constant value of Y, say $Y_{cl}$ where, by using eqs. (61,47,64 and 65), $Y_{cl}$ is readily found to be given by

$$Y_{cl} = \frac{\alpha_{xx}}{\beta_{xx}} \frac{\zeta_{cl} - \zeta_m}{\zeta_m - \zeta_{th}} \quad . \tag{A5}$$

Similarly the locus in the Y vs X plot corresponding to the angular momentum where the fission barrier vanishes is given by the horizontal line

$$Y = Y(0) \tag{A6}$$

and, more generally, the locus where the fission barrier has reached some prescribed value $B_f$ is given by

$$Y = Y(B_f) \quad . \tag{A7}$$

In the above, $Y(0)$ and $Y(B_f)$ are numbers that may be estimated (for a rotating liquid drop) by using Ref. 29. Thus,

$$Y(B_f) = \frac{E\sigma}{\pi r^2} = \frac{E\pi b^2}{\pi r^2} = \frac{L^2}{2M_r r^2} \quad .$$

Using the relation between $L^2$ and y provided by eq. (50) we find

$$Y(B_f) = \frac{2}{5}\left(\frac{M}{M_r}\right)\left(\frac{R}{r}\right)^2 (4\pi R^2\gamma)y = \frac{2}{5}\left(\frac{r_o}{r}\right)^2 (4\pi r_o^2\gamma)\frac{A^{10/3}}{A_1A_2}\, y \quad . \tag{A8}$$

In the above equations, A, M, R refer to the mass number, mass, and radius of the spherical configuration and the parameter y is the conventional liquid-drop rotational parameter. Since y is proportional to the rotational energy of a rigid sphere, it is related to the variable Y (the orbital energy at contact) by a simple geometrical factor, consisting of the quotient of the relevant moments of inertia.

The fission barrier of a rotating drop specified by a fissility parameter x and a rotation parameter y may be estimated from Figs. 12 and 13 in Ref. 29. In particular, the value of y (or of the angular momentum) at which the fission barrier vanishes is defined by the curve $y_{II}(x)$ in Fig. 2 of that reference. An approximation to this curve may be written as

$$y_{II} = 1.228(0.64 - x) + 0.0000487e^{x/0.0868} \quad \text{for } 0 \leqslant x \leqslant 0.637$$

$$y_{II} = 0.0280 - 0.2225(x - 0.81) + 0.405(x - 0.81)^2 \quad \text{for } 0.637 \leqslant x \leqslant 0.81) \tag{A9}$$

$$y_{II} = \frac{7}{5}(1 - x)^2 - 4.566(1 - x)^3 + 6.7443(1 - x)^4 \quad \text{for } 0.81 \leqslant x \leqslant 1$$

We recall the numerical formulae for x and y that follow from using the parameters of Ref. 9

$$x = \frac{Z^2/A}{50.883(1 - 1.7826I^2)} \tag{A10}$$

$$y = \frac{1.9407\ \ell^2}{(1 - 1.7826I^2)A^{7/3}} \quad . \tag{A11}$$

The conventional plots of the cross section $\sigma$ vs the energy E (e.g. Fig. 6) may be considered as distorted images of the rectilinear plots in Fig. 9 (where Y can be thought of as a measure of cross section and X as a measure of the (radial) energy excess over the barrier). The energies corresponding to the intersections of the various straight lines in Fig. 9 are readily written down and the following formulae may be verified trivially. For example, in Fig. 9a, one finds

$E_1 - B = -\alpha_x/\beta_x$ = energy excess over barrier at which deep-inelastic reactions appear for the highest impact parameters in cases when $\alpha_x$ is negative, (A12)

$E_2 - B = Y_{c1} + (\alpha_x + \beta_x Y_{c1})^2$ = energy excess over barrier at which the entrance-channel limitation on compound-nucleus formation first appears for the highest impact parameters and the cross section begins to decrease. (A13)

$E_3 - B = Y_{cl} + (\alpha_{xx} + \beta_{xx} Y_{cl})^2$ = energy excess over the barrier at which the above limitation begins to be overcome by an increasing number of partial waves and the compound-nucleus cross section begins to increase once again. (A14)

Similarly, in Fig. 9b, we find

$E_4 - B = \alpha_x^2$ = energy excess over barrier at which the extra push is overcome in head-on collisions and fusion begins, (A15)

$E_5 - B = \alpha_{xx}^2$ = energy excess over barrier at which the extra-extra push is overcome in head-on collisions and compound-nucleus formation begins. (A16)

In the same way, the energies corresponding to the intersection of any other pair of lines in Fig. 9 may be written down by inspection using eqs. (A1-A7).

The simplicity of the rectilinear cross-section plots and their direct relation to theoretical concepts suggests that it might often be advantageous to present experimental data by plotting Y vs X, in addition to $\sigma$ vs E. Still, the advantage of the conventional plots is that they are truly model independent and represent the raw data. In a plot of Y vs X one has to commit oneself to some values of the contact energy B and the contact distance r (as given, for example, by semi-empirical expressions). If, however, the cross-section data for a given reaction are sufficiently precise and extensive in the vicinity of the barrier, then B and r for the system under consideration may be deduced empirically (from the intercept and slope of the excitation function) and the plot of Y vs X also becomes, in effect, model independent.

TABLE I

Estimates of Parameters

| | Empirical | Schematic Model (Ref. 12) | Improved Model |
|---|---|---|---|
| Threshold fissility parameter $x_{th}$ | $0.70 \pm 0.02$ | 0.584 | $\approx 0.723$* |
| Threshold coefficient b | $35.62 \pm 1$ | -- | $\approx 36.73$ |
| Slope coefficient a | $12 \pm 2$ | 5 | $\approx 18$* (or less**) |
| Angular momentum fraction f | $\frac{3}{4} \pm 10\%$ | $0.85 \pm 0.02$*** | --- |
| Cliff constant k | --- | $k = 1$ | --- |
| Cliff fissility parameter $x_{cl}$ | $(0.84 \lesssim x_{cl} \lesssim 0.86?)$ | 0.70 | --- |
| Cliff coefficient c | $(42.7 \lesssim c \lesssim 43.8?)$ | --- | --- |

*Deduced from J. Blocki et al., private communication, 1981

**H. Feldmeier, Ref. 26 and private communication, 1982, see text

***G. Fai, private communication, 1981, to be published

TABLE II

| x | $\eta(x)$ | $f_m$ for $A_1/A_2=1$ | $f_m$ for $A_1/A_2=8$ |
|---|---|---|---|
| 0 | 1.2723 | 0.7375 | 0.5158 |
| 0.05 | 1.3111 | 0.7431 | 0.5197 |
| 0.1 | 1.3569 | 0.7495 | 0.5242 |
| 0.15 | 1.4120 | 0.7570 | 0.5294 |
| 0.2 | 1.4793 | 0.7658 | 0.5356 |
| 0.25 | 1.5632 | 0.7765 | 0.5431 |
| 0.3 | 1.6704 | 0.7894 | 0.5521 |
| 0.35 | 1.8113 | 0.8056 | 0.5634 |
| 0.4 | 2.0026 | 0.8261 | 0.5778 |
| 0.45 | 2.2726 | 0.8526 | 0.5963 |
| 0.5 | 2.6684 | 0.8875 | 0.6207 |
| 0.55 | 3.2603 | 0.9331 | 0.6526 |
| 0.6 | 4.0796 | 0.9869 | 0.6902 |
| 0.65 | 4.7318 | 1.0242 | 0.7163 |
| 0.7 | 5.2287 | 1.0501 | 0.7344 |
| 0.76 | 5.8400 | 1.0795 | 0.7550 |
| 0.8 | 6.6082 | 1.1134 | 0.7787 |
| 0.85 | 7.6907 | 1.1564 | 0.8088 |
| 0.9 | 9.8927 | 1.2315 | 0.8614 |
| 0.95 | 16.8271 | 1.4064 | 0.9837 |
| 1.0 | $\infty$ | $\infty$ | $\infty$ |

TABLE III

| Reaction | $B^*_{exp}$ | 0.96 $B_{Prox}$ | $B_{exp}$ - 0.96 $B_{Prox}$ | $\Delta B_{theory}$ =0, or $K(\zeta_e-\zeta_{th})^2$ | $\zeta_e-\zeta_{th}$ |
|---|---|---|---|---|---|
| $^{40}Ar_{18}$ + $^{206}Pb_{82}$ | 162 ± 3 | 158.95 | 3.05 ± 3 | 0 | -2.0545 |
| $^{50}Ti_{22}$ + $^{208}Pb_{82}$ | 191 ± 3 | 190.14 | 0.86 ± 3 | 1.17 | 1.1703 |
| $^{50}Ti_{22}$ + $^{208}Bi_{83}$ | 190 ± 3 | 192.38 | -2.38 ± 3 | 1.65 | 1.3878 |
| $^{86}Kr_{36}$ + $^{123}Sb_{51}$ | 209.4 ± 3 | 197.77 | 11.63 ± 3 | 3.29 | 1.8018 |
| $^{94}Zr_{40}$ + $^{124}Sn_{50}$ | 219.3 ± 3 | 213.00 | 6.30 ± 3 | 11.41 | 3.3214 |
| $^{76}Ge_{32}$ + $^{170}Er_{68}$ | $242^{+\infty}_{-5}$ | 227.00 | $15.00^{+\infty}_{-5}$ | 20.63 | 4.5475 |
| $^{86}Kr_{36}$ + $^{160}Gd_{64}$ | ⩾260 | 239.30 | ⩾20.70 | 33.27 | 5.6755 |
| $^{110}Pd_{46}$ + $^{136}Xe_{54}$ | ⩾283 | 256.45 | ⩾26.55 | 56.00 | 7.1944 |

*Ref. 30

TABLE IV

A comparison of three super-heavy element reactions, $^{248}Cu + ^{48}Ca$, $^{252}Cf + ^{48}Ca$, and $^{254}Es + ^{48}Ca$, with the calibrating reaction $^{209}Bi + ^{54}Cr$

| | | Bi + Cr | Cm + Ca | Cf + Ca | Es + Ca |
|---|---|---|---|---|---|
| Estimated barrier in MeV (0.96 $B_{prox}$): | C.M. | 208.66 | 196.54 | 200.14 | 201.94 |
| | Lab | 262.57 | 234.58 | 238.26 | 240.10 |
| Lab energies used | | 261.9<br>267.3 | --- | --- | --- |
| Q-value | | 191.47 | 170.93 | 174.01 | 175.59 |
| Excitation following reaction at nominal barrier | | 17.19 | 25.61 | 26.13 | 26.35 |
| Excitation in experiments | | 16.66<br>20.95 | --- | --- | --- |
| Estimated bindings: (Ref. 5) | First neutron | 6.69 | 7.58 | 7.73 | 6.49 |
| | Second neutron | 8.16 | 6.26 | 6.42 | 7.82 |
| Expected reactions | | 1n(2n) | 2n(3n) | 2n(3n) | 2n(3n) |
| Estimated fission barrier before neutron emissions | | ∿ 3 - 4 | ∿ 5.6 ? | ∿ 7.0 ? | ∿ 7.6 ? |
| Even-even lifetime after neutron emissions (Ref. 36) | Fission | ? | $10^{-17}$ y | $10^{-13}$ y | $10^{-11}$ y |
| | Alpha | $4 \times 10^{-10}$ y* | $10^{-9}$ y | $10^{-9}$ y | $10^{-10}$ y |
| Odd-odd enhancement | | Yes | No | No | Yes |
| Ground-state deformation | | Yes | No | No | No |
| Fissility $Z^2/A$ | | 43.532 | 45.459 | 46.413 | 46.891 |
| Entrance-channel fissility $(Z^2/A)_{eff}$ | | 36.567 | 33.917 | 34.323 | 34.524 |

*odd-odd, experimental

TABLE IV (continued)

| | | Bi + Cr | Cm + Ca | Cf + Ca | Es + Ca |
|---|---|---|---|---|---|
| Geometric mean fissility $(Z^2/A)_g$ | | 39.898 | 39.266 | 39.913 | 40.235 |
| Cost in MeV of side-step reaction | | 0.96 | 5.04 | 3.84 | 1.52 |
| $(Z^2/A)_{eff}$ for side-step reaction | | 35.466 | 32.557 | 32.940 | 33.129 |
| $(Z^2/A)_g$ for side-step reaction | | 39.293 | 38.471 | 39.100 | 39.414 |
| Cost of double side step | | 1.70 | 2.35 | 2.27 | 2.68 |
| Energy resulting in excitation of 20.95 MeV | C.M. | 212.42 | 191.88 | 194.96 | 196.54 |
| | Lab | 267.30 | 229.02 | 232.10 | 233.68 |
| Energy resulting in excitation of 16.16 MeV | C.M. | 208.13 | 187.09 | 190.17 | 191.75 |
| | Lab | 261.91 | 223.30 | 226.39 | 227.97 |
| Even-even lifetime after one neutron emission | Fission | ? | $10^{-14}$ y | $10^{-10}$ y | $10^{-8}$ y |
| | Alpha | $4 \times 10^{-10}$ y* | $10^{-7}$ y | $10^{-8.5}$ y | $10^{-10}$ y |
| Odd-odd or odd-A enhancement | | Yes | Yes | Yes | Yes |

## References


1. W.J. Swiatecki, "The Nature of Nuclear Dynamics", Proceedings Workshop on Nuclear Dynamics, 22-26 February 1982, Granlibakken, Lawrence Berkeley Laboratory preprints LBL-14138, April 1982, and LBL-14073, April 1982.
2. W.J. Swiatecki, Prog. Particle and Nucl. Physics 4 (1980) 383.
3. W.D. Myers and W.J. Swiatecki, Annals of Phys. 55 (1969) 395.
4. W.D. Myers and W.J. Swiatecki, Nucl. Phys. 81 (1966) 1, especially sections 3,4.
5. W.D. Myers, "Droplet Model of Atomic Nuclei", IFI/Plenum, 1977.
6. V.M. Strutinskii and A.S. Tyapin, Zhur. Eksp. i Teoret. Fiz. 45 (1963) 960.
7. W.D. Myers and W.J. Swiatecki, "The Macroscopic Approach to Nuclear Masses and Deformations", Lawrence Berkeley Laboratory preprint LBL-13929, 1982, to appear in Advances in Nuclear Physics.
8. M. Brack, J. Damgaard, A.S. Jensen, H.C. Pauli, V.M. Strutinskii, and C.Y. Wong, Rev. Mod. Phys. 44 (1972) 320.
9. W.D. Myers and W.J. Swiatecki, Proc. Lysekil Symposium 1966, Ark. Phys. 36 (1967) 343.
10. J. Blocki, Y. Boneh, J.R. Nix, J. Randrup, M. Robel, A.J. Sierk, and W.J. Swiatecki, Annals of Phys. 113 (1978) 330.
11. J. Randrup and W.J. Swiatecki, Annals of Phys. 125 (1980) 193.
12. W.J. Swiatecki, Physica Scripta 24 (1981) 113.
13. D.L. Hill and J.A. Wheeler, Phys. Rev. 89 (1953) 1102.
14. J.R. Nix and A.J. Sierk, Phys. Rev. C21 (1980) 396 and Refs. 10-30 therein.
15. J.R. Nix and A.J. Sierk, Phys. Rev. C21 (1980) 982.
16. References 9-12 in H.C. Britt, B.H. Erkkila, A. Gavron, Y. Patin, R.H. Stokes, M.P. Webb, P.R. Christensen, O. Hansen, S. Pontoppidan, F. Videbaek, R.L. Ferguson, F. Plasil, G.R. Young, and J. Randrup, Los Alamos preprint LA-UR-82-700 (1982), submitted to Phys. Rev. C.

17. W.J. Swiatecki, Nucl. Phys. A376 (1982) 275.

18. W.J. Swiatecki, Proc. 4th International Conference on Nuclei Far from Stability, Helsingør, June 7-13, 1981, P.G. Hansen, editor.

19. H. Sann, R. Bock, Y.T. Chu, A. Gobbi, A. Olmi, U. Lynen, W. Müller, S. Bjørnholm, and H. Esbensen, Phys. Rev. Lett. 47 (1981) 1248.

20. R. Bock, Y.T. Chu, M. Dakowski, A. Gobbi, E. Grosse, A. Olmi, H. Sann, D. Schwalm, U. Lynen, W. Müller, S. Bjørnholm, H. Esbensen, W. Wölfli, and E. Morenzoni, Nucl. Phys. A (1982), to appear.

21. B. Sikora, J. Bisplinghoff, M. Blann, W. Scobel, M. Beckerman, F. Plasil, R.L. Ferguson, J. Birkelund, and W. Wilcke, Phys. Rev. C25 (1982) 686, and private communication from M. Blann.

22. R.A. Esterlund, W. Westmeier, A. Rox, and P. Patzelt, contribution to International Conference on Selected Aspects of Heavy Ion Reactions, Saclay, 3-7 May, 1982.

23. J.R. Nix and A.J. Sierk, Phys. Rev. C15 (1977) 2072.

24. R. Bass, Nucl. Phys. A231 (1974) 45.

25. J. Blocki and W.J. Swiatecki, "Nuclear Deformation Energies", LBL-12811, in preparation.

26. F. Beck, J. Blocki, and H. Feldmeier, Proc. Int. Workshop on Gross Properties of Nuclei and Nuclear Excitations X, Hirschegg, Jan. 18-22, 1982.

27. J.R. Huizenga, J.R. Birkelund, W.V. Schröder, W.W. Wilcke, and H.J. Wollersheim in "Dynamics of Heavy-Ion Collisions", N. Cindro, R.A. Ricci, and W. Greiner (editors), North-Holland Publishing Co., 1981, p. 15.

28. G. Fai, private communication, 1982, to be published.

29. S. Cohen, F. Plasil, and W.J. Swiatecki, Annals of Phys. 82 (1974) 557.

30. H. Gäggeler, W. Brüchle, J.V. Kratz, M. Schädel, K. Sümmerer, G. Wirth, and T. Sikkeland, Proc. Int. Workshop on Gross Properties of Nuclei and Nuclear Excitations X, Hirschegg, Jan. 18-22, 1982.

31. L.C. Vaz, J.M. Alexander, and G.R. Satchler, Phys. Reports 69, (1981) 373, Fig. 5.

32. J.V. Kratz, "The Search for Superheavy Elements", preprint GSI-82-7, February 1982, submitted to Radiochemica Acta.

33. A. Gobbi, G. Guarino, J.V. Kratz, A. Olmi, K. Sümmerer, G. Wirth, C. Gregoire, R. Lucas, J. Poitou, and S. Bjørnholm, Proc. Int. Workshop on Gross Properties of Nuclei and Nuclear Excitations X, Hirschegg, Jan. 18-22, 1982.

34. G. Münzenberg, S. Hofmann, F.P. Hessberger, W. Reisdorf, K.-H. Schmidt, J.R.H. Schneider, P. Armbruster, C.C. Sahm, and B. Thuma, Z. Phys. A300 (1981) 107.

35. G. Münzenberg, S. Hofmann, F.P. Hessberger, W. Reisdorf, K.-H. Schmidt, J.R.H. Schneider, J.-J. Schött, P. Armbruster, C.C. Sahm, D. Vermeulen, and B. Thuma, GSI Annual Report 1981.

36. J. Randrup, S.E. Larsson, P. Möller, A. Sobiczewski, and A. Lukasiak, Physica Scripta 10A (1974) 60.

37. K.-H. Schmidt, W. Faust, G. Münzenberg, W. Reisdorf, H.-G. Clerc, D. Vermeulen, and W. Lang, Proc. 4th IAEA Symp. on Physics and Chemistry of Fission, Jülich, 1979 (IAEA, Vienna, 1980) Vol. I, p. 409.

38. J.G. Keller, H.-G. Clerc, D. Vermeulen, and K.-H. Schmidt, preprint IKDA 81/7, Darmstadt, Aug. 1981.

39. C.C. Sahn, H.-G. Clerc, D. Vermeulen, K.-H. Schmidt, P. Armsbruster, F. Hessberger, J. Keller, G. Münzenberg, and W. Reisdorf, Proc. Xth Workshop on Gross Properties of Nuclei and Nuclear Excitations, Hirschegg, Jan. 18-22, 1982.

## Figure Captions

Fig. 1. Schematic illustration of the relation between three critical energies, four types of nuclear reactions, and two kinds of extra push. This figure is appropriate when the three milestone configurations discussed in the text exist and are distinct. In some situations the critical energies I,II,III may merge (pairwise or all together) squeezing out the regimes corresponding to Dinucleus and/or Mononucleus Reactions. In other situations one or both of the upper boundaries (II and III) may dissolve, making the adjoining regions merge into continuously graduated reaction types.

Fig. 2a. Contour lines of the estimated extra push (in MeV) over the interaction barrier, needed to overcome the conditional saddle (i.e. the saddle at frozen asymmetry). For asymmetric systems and an injection energy beyond about the 10 MeV contour the conditional saddle begins to lose its physical significance because of the unfreezing of the asymmetry. The figure refers to the schematic model and must not be used for actual estimates.

Fig. 2b. Contour lines (in MeV) of the estimated extra-extra push over the interaction barrier needed to make a compound nucleus (or, at least, to form a spherical composite nucleus) out of two nuclei with atomic numbers $Z_1$ and $Z_2$. (Schematic model, not be be compared with experiment.)

Fig. 2c. Contour lines of equal extra-extra push $E_{xx}$, using analytic scaling formula fitted to schematic model.

Fig. 3. Contour lines of the extra push according to eq. (41), with parameters adjusted to reproduce the data of Ref. 20.

Fig. 4. Contour lines of equal extra-extra push. In the region below the cliff the contour lines are identical with the extra push in Fig. 3. Above the cliff, eq. (42) was used, with k = 1, $x_{cl}$ = 0.84. Since neither k nor $x_{cl}$ has been determined experimentally, the location and height of the cliff are given for illustrative purposes only. Also, the cliff is not expected to be sharp but should come in with a finite degree of abruptness, whose extent is not known. In the region of the "Thud Wall", the extra-extra push rises to very high values.

Fig. 5. The excitation functions for various types of reactions. Figure 5(a) illustrates the qualitative distinction between binary (elastic and quasi-elastic) reactions, dinucleus (deep-inelastic) reactions, mononucleus (fast-fission) reactions, and compound nucleus reactions. The latter divide into (delayed) fission reactions and evaporation residue reactions. Some characteristic lifetimes (in seconds) are indicated on the right. The dotted curve illustrates qualitatively the additional entrance-channel limitation on compound-nucleus formation resulting from the requirement of an extra-extra push to reach the vicinity of the spherical shape. Figures 5(b),(c),(d) show a comparison of theory and experiment for three cases. The triangles refer to evaporation-residue cross sections, to be compared with the triple-dot-dashed curves. The circles have had cross sections for fission-like events added and are to be compared with the dashed curves. There are considerable uncertainties in both theory and measurement. In particular, the distinction between deep-inelastic and fission-like events is expected to become blurred at the higher energies, and the dashed

curves should be imagined as fading out towards the right. The labels along the dashed curves refer to the generalized fissility parameter $x_e(\ell)$. The labels $B_f = 0$, $B_f \approx B_n$, $B_f$ $(L = 0)$ refer to loci along which the fission barrier (of a rotating, idealized drop) has the value zero, or is about equal to the neutron binding energy, or has its full value corresponding to zero angular momentum.

Fig. 6. This is like Fig. 5 but for a set of seven reactions with heavier systems. The parameters of the theory ($x_{th} = 0.70 \pm 0.02$, $a = 12 \pm 2$, $f = 0.75 \pm 10\%$) were fitted to these data and used without modification in Fig. 5. The dotted curves, corresponding to the entrance-channel, extra-extra push limitation, are for illustrative purposes only--their actual positions are unknown.

Fig. 7. A comparison of theory and experiment concerning the need for an extra push to form compound nuclei. The experimental points and lower limits are obtained by taking the difference between effective barriers (that have to be inserted in a standard theory to reproduce xn excitation functions) and baseline barriers estimated from smooth systematics representing average behaviour for not too heavy systems (where no extra push is expected). The curve shows the trend of the theoretical extra-push prediction (corresponding to the parameters fitted to Fig. 6). There are considerable uncertainties both in the experimental points and in the baseline barriers that affect the comparison.

Fig. 8. A comparison, along the lines of Figs. 5 and 6, of the superheavy candidate reaction $^{248}Cm + ^{48}Ca$, with the calibrating reaction $^{209}Bi + ^{54}Cr$, in which element 107 was produced. (Three atoms at each of the two center-of-mass energies indicated by the arrows.) The extra- and extra-extra push limitations are comparable in the two systems. The former is, in fact, a little less severe for $^{248}Cm + ^{48}Ca$, making it likely that a superheavy mononucleus will be formed at bombarding energies in the vicinity of the estimated interaction barrier (196.5 MeV in the center of mass). Whether a compound nucleus will be formed with reasonble cross section is more problematic. Whether it will survive fission will depend on how large and how excitation-resistant is the anticipated shell effect. Whether a superheavy nucleus will be detected will depend additionally on the sensitivity and lifetime range of the experimental techniques.

Fig. 9. An illustration of the simplicity of the rectilinear cross-section plots, in which the quantity Y ($\equiv \sigma E/\pi r^2$) is plotted against X [$\equiv\sqrt{E-B-(\sigma E/\pi r^2)}$]. The plots may be thought of as rectified excitation-function plots of $\sigma$ vs E, with the vertical Y-axis corresponding to the standard reaction cross section $\sigma = \pi r^2(1 - B/E)$, and the sloping or horizontal lines to excitation functions limited by the extra push, the extra-extra push, or by a limiting angular momentum. Simple formulae follow for the energies (and cross sections) corresponding to the critical intersection points, some of which are indicated by circled numbers. The quantity Y is the orbital energy at contact and $X^2$ is the radial energy at contact. Loci of constant (bombarding) energy (not shown) are parabolas corresponding to $Y + X^2$ = constant.

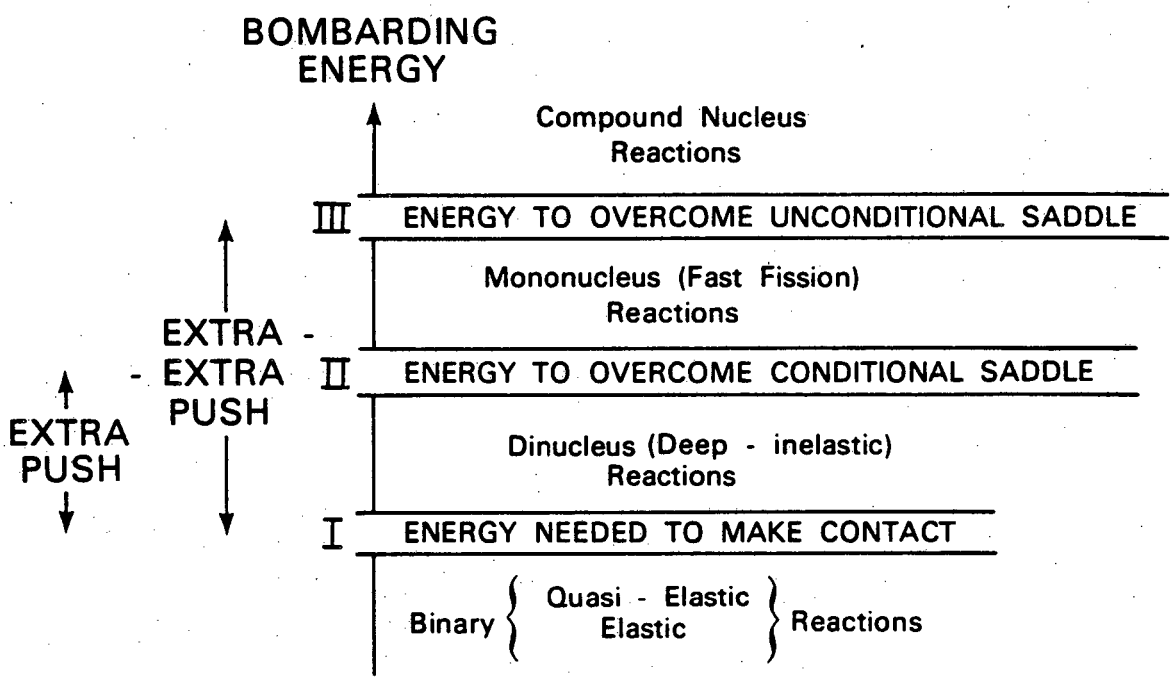


Figure 1

XBL 823-192

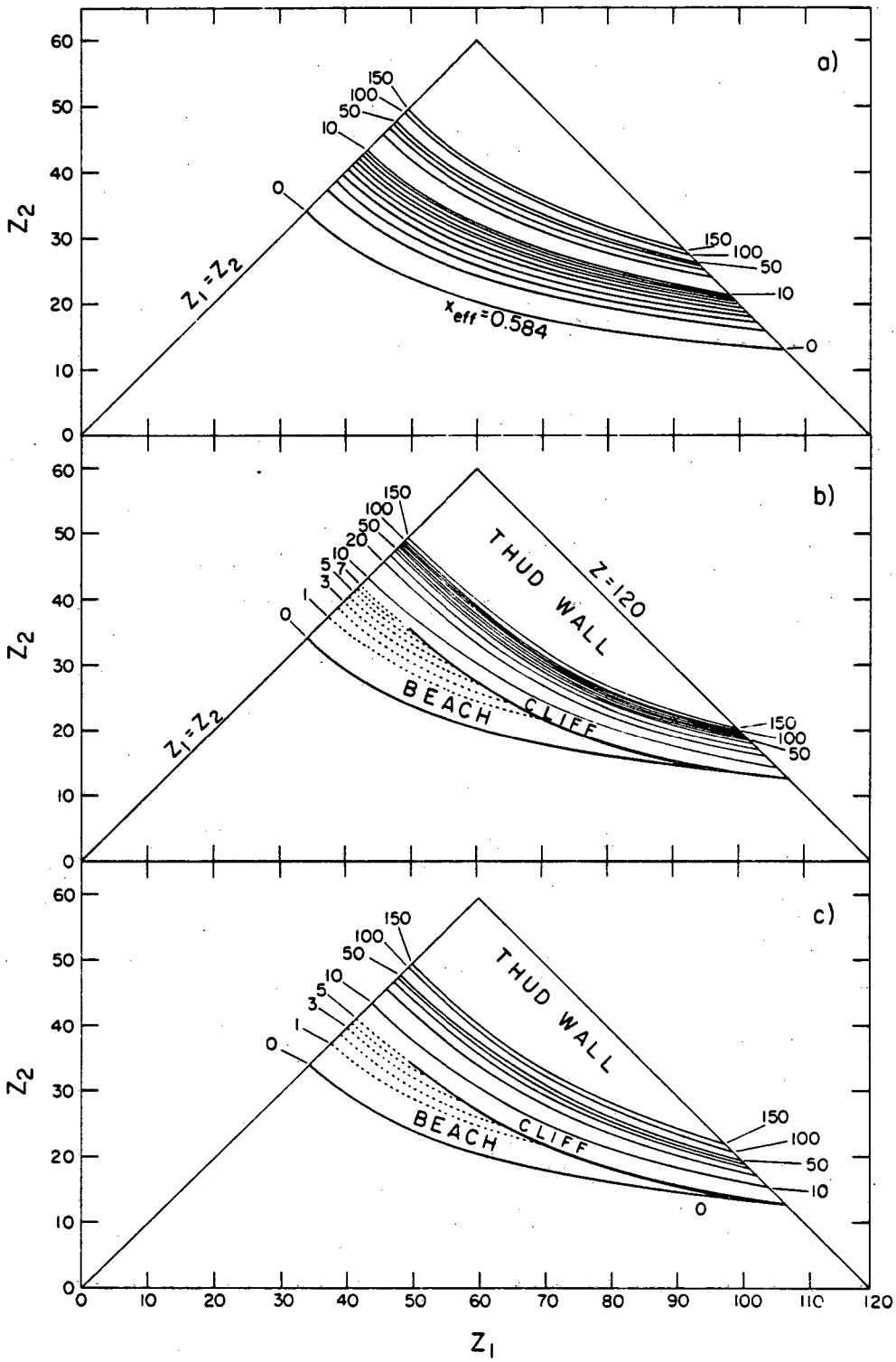


Figure 2

XBL 823-189

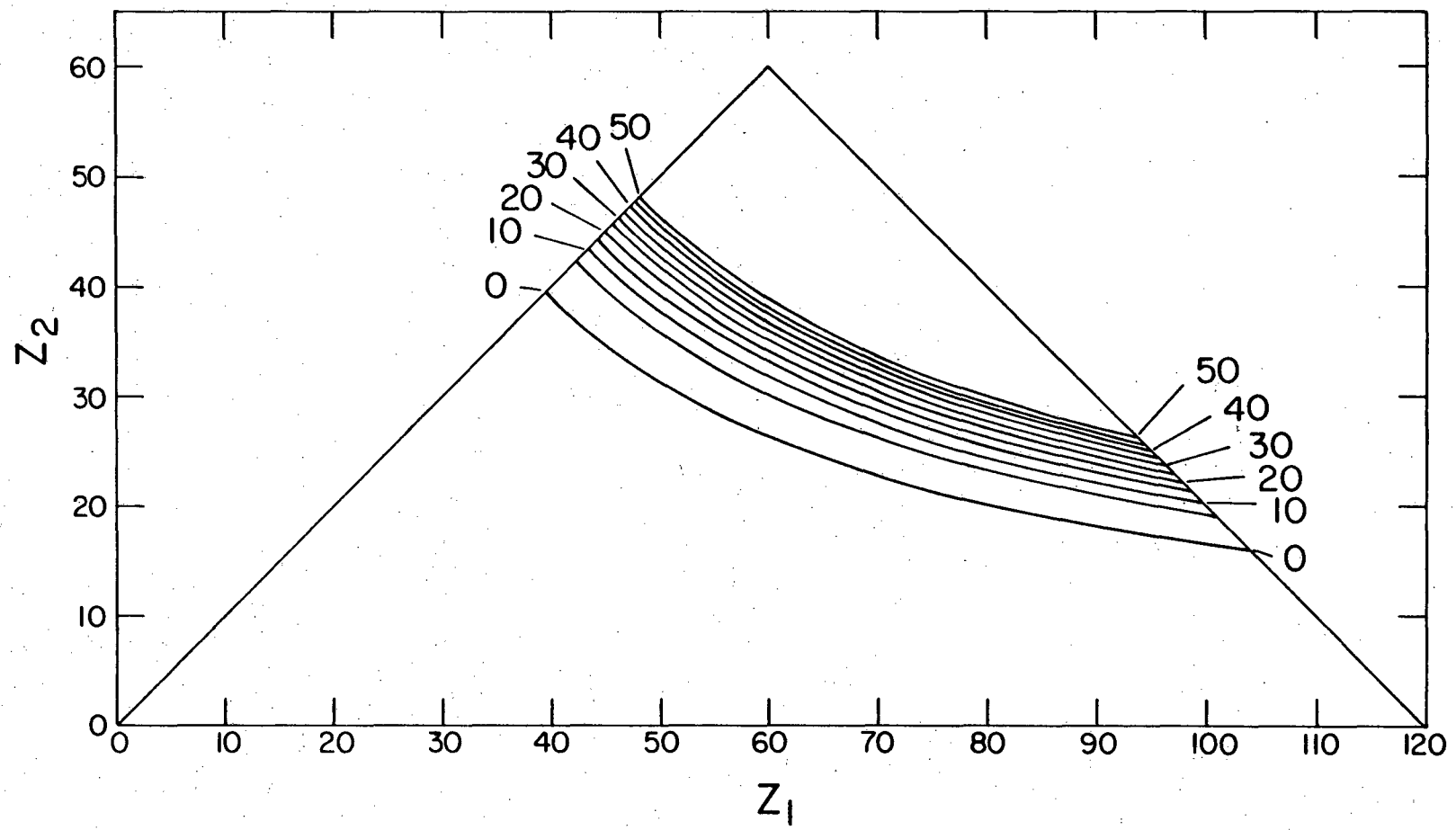


Figure 3

XBL 823-184

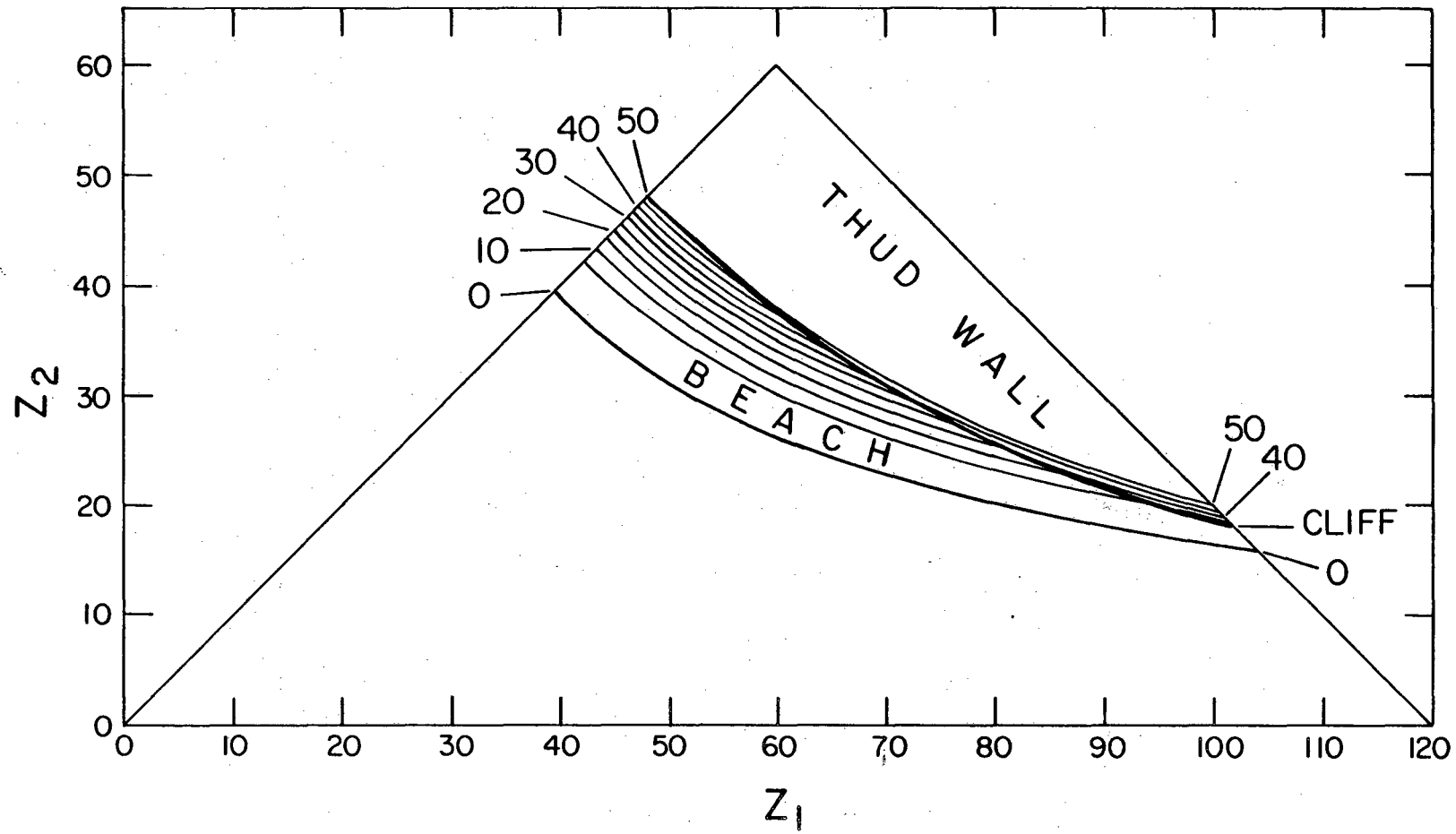


Figure 4

XBL 823-188

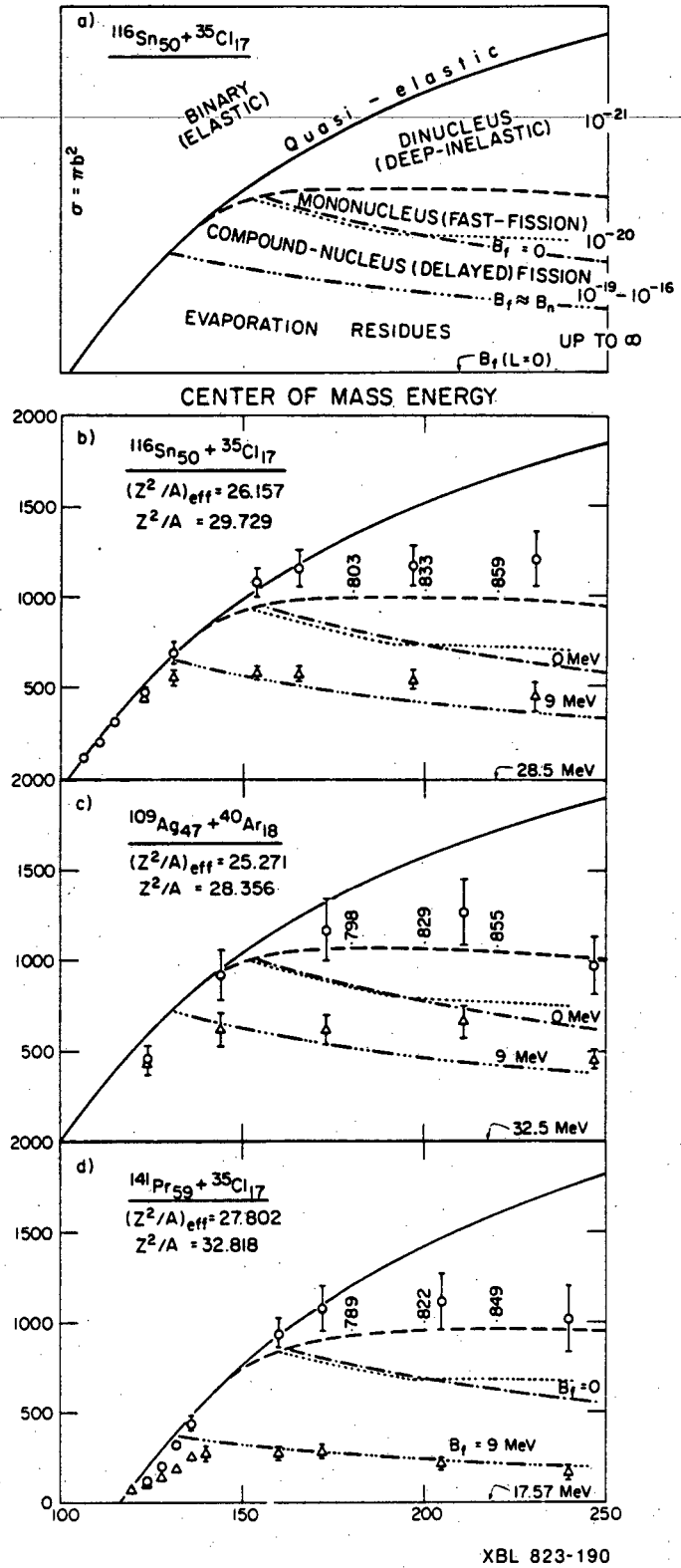


XBL 823-190

Figure 5

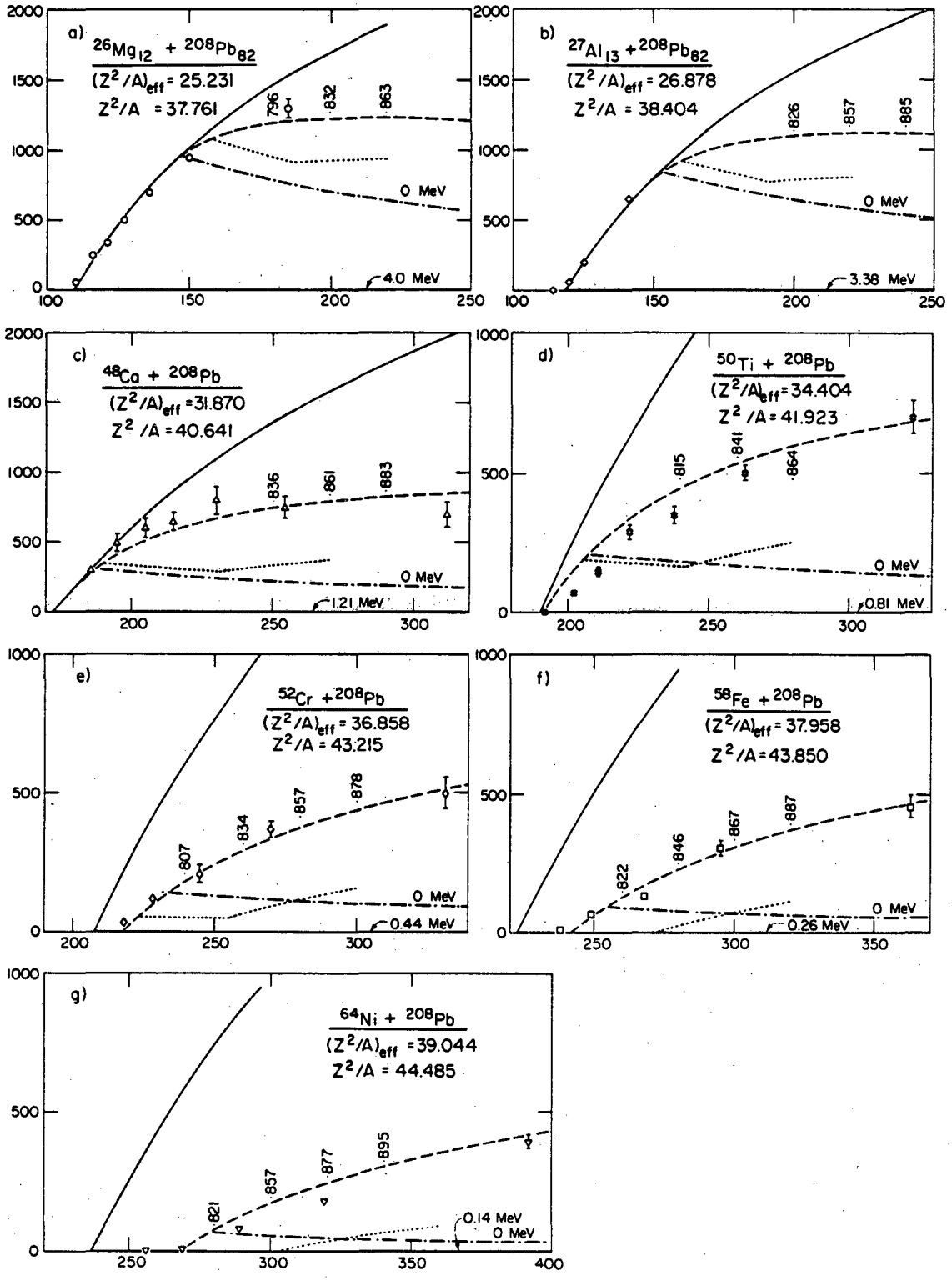


XBL 823-191

Figure 6

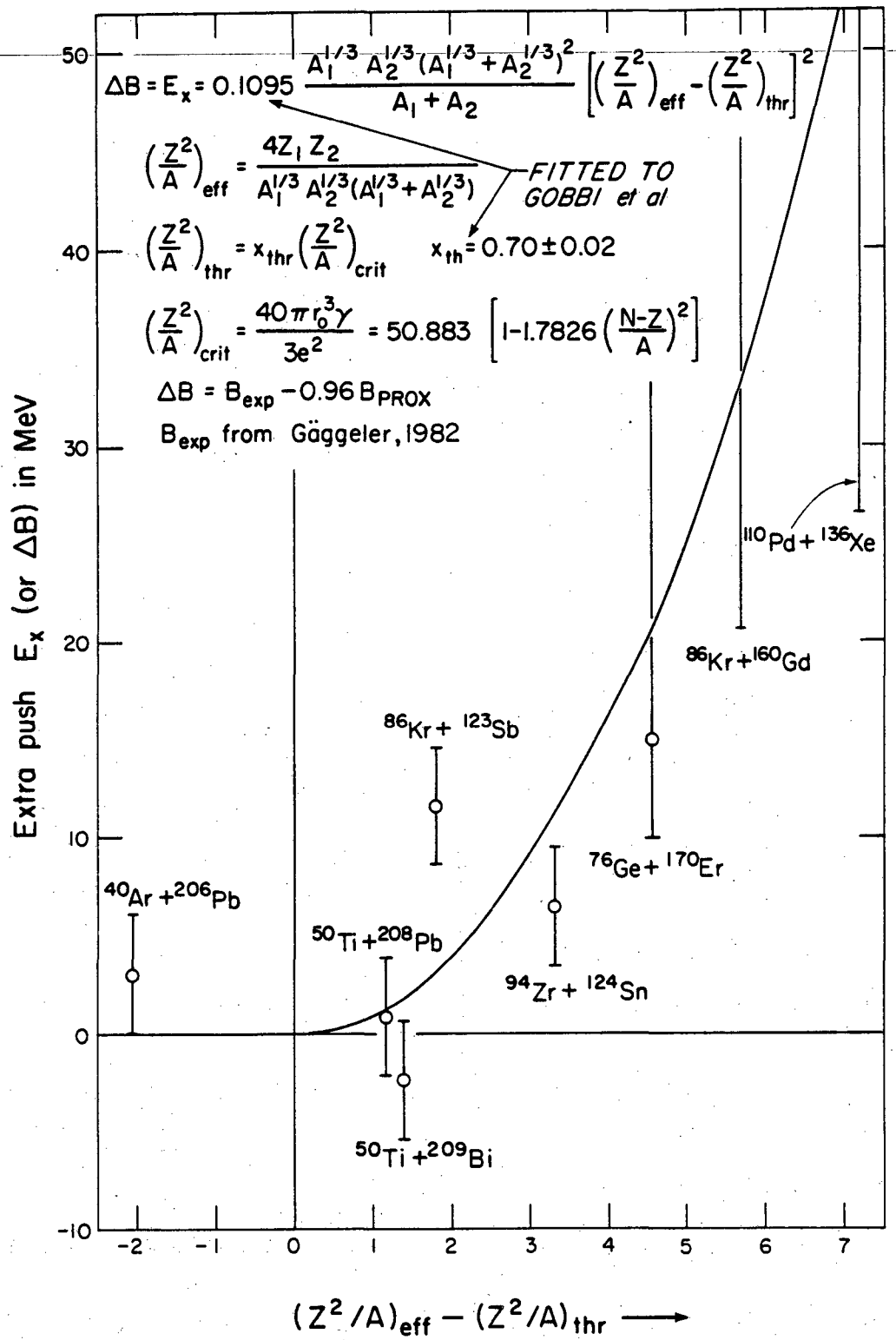


Figure 7

XBL 823-187

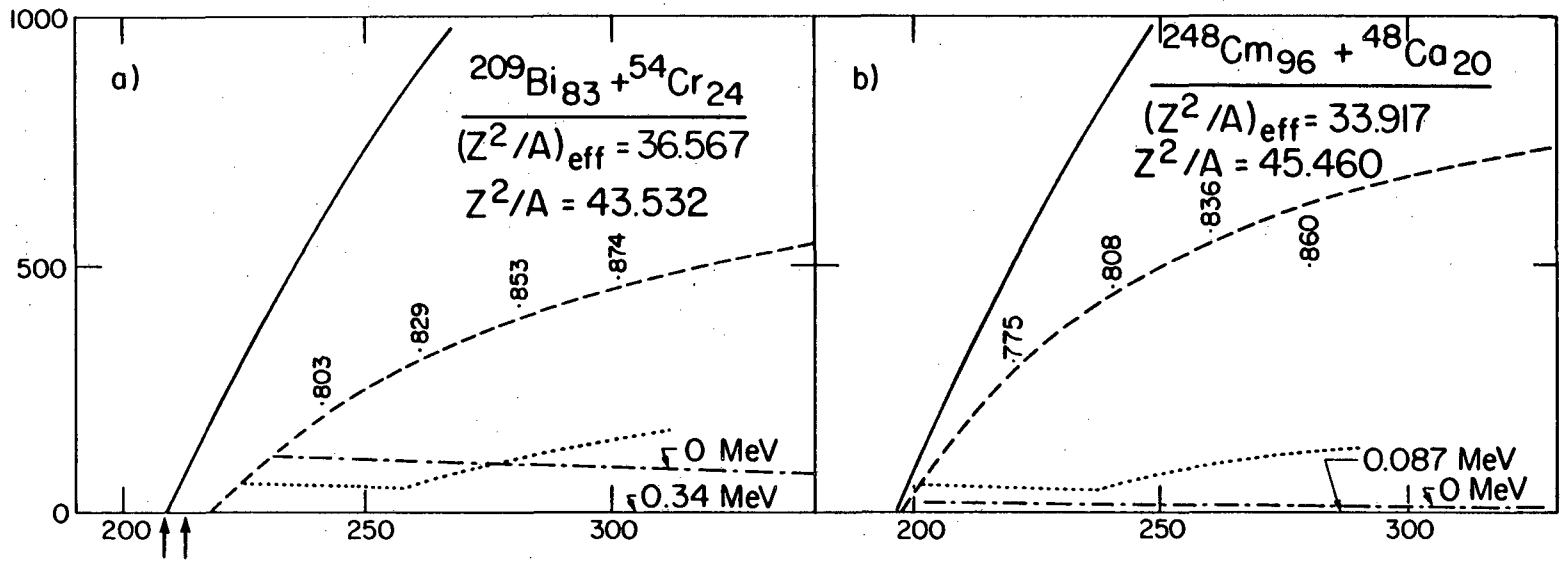
1000
500
0
200
250
300
a)
$^{209}Bi_{83} + ^{54}Cr_{24}$
$(Z^2/A)_{eff} = 36.567$
$Z^2/A = 43.532$
.803
.829
.853
.874
0 MeV
0.34 MeV
b)
$^{248}Cm_{96} + ^{48}Ca_{20}$
$(Z^2/A)_{eff} = 33.917$
$Z^2/A = 45.460$
.775
.808
.836
.860
0.087 MeV
0 MeV
XBL 823-185

Figure 8

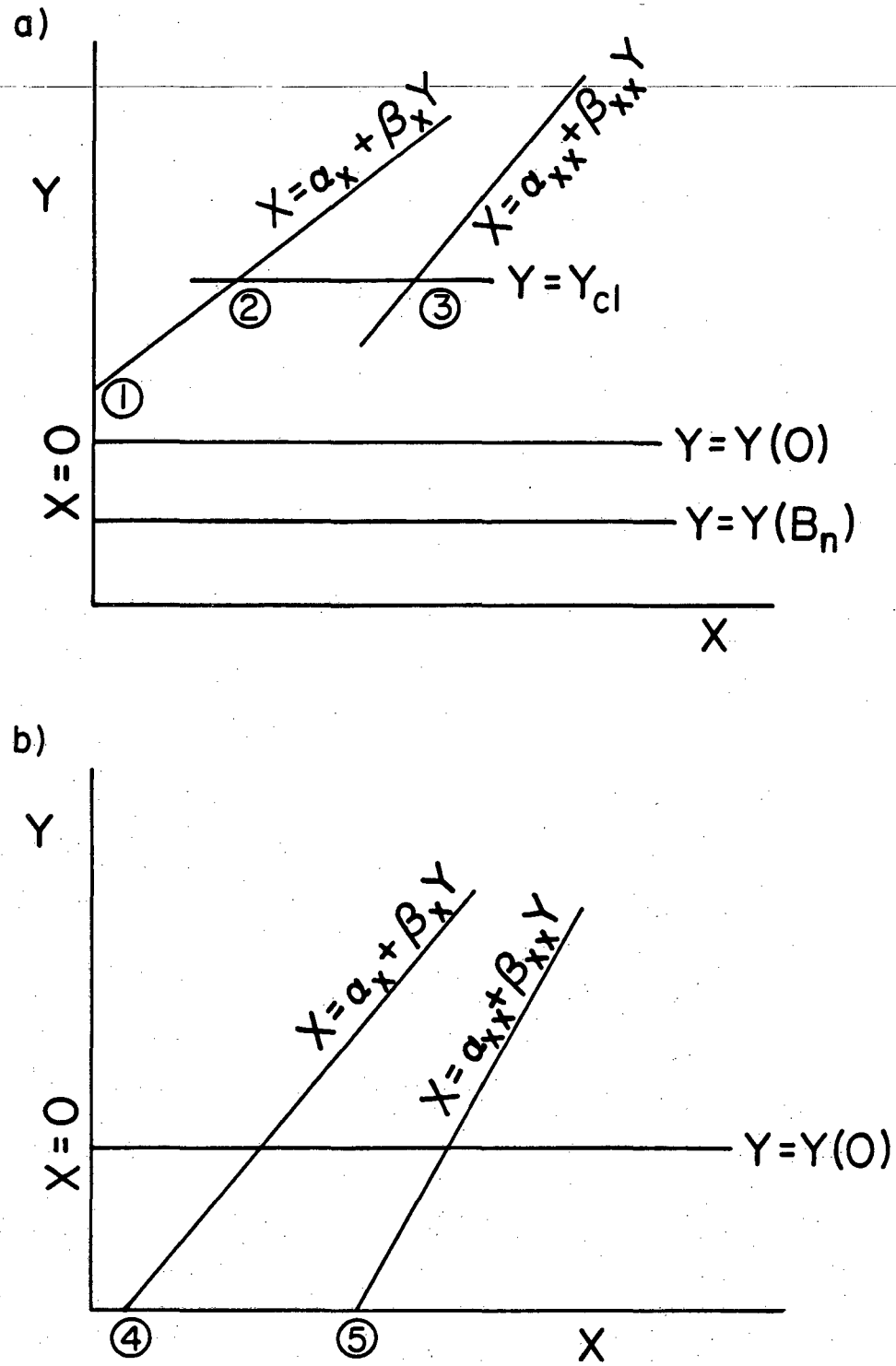


Figure 9

XBL 823-284

This report was done with support from the Department of Energy. Any conclusions or opinions expressed in this report represent solely those of the author(s) and not necessarily those of The Regents of the University of California, the Lawrence Berkeley Laboratory or the Department of Energy.

Reference to a company or product name does not imply approval or recommendation of the product by the University of California or the U.S. Department of Energy to the exclusion of others that may be suitable.

*TECHNICAL INFORMATION DEPARTMENT*
*LAWRENCE BERKELEY LABORATORY*
*UNIVERSITY OF CALIFORNIA*
*BERKELEY, CALIFORNIA 94720*